

A Catalog of Transient X-ray Sources in M31

Benjamin F. Williams^{1,2}, S. Naik^{3,4}, Michael R. Garcia¹, Paul J. Callanan³

ABSTRACT

From October 1999 to August 2002, 45 transient X-ray sources were detected in M31 by *Chandra* and *XMM-Newton*. We have performed spectral analysis of all *XMM-Newton* and *Chandra* ACIS detections of these sources, as well as flux measurements of *Chandra* HRC detections. The result is absorption-corrected X-ray lightcurves for these sources covering this 2.8 year period, along with spectral parameters for several epochs of the outbursts of most of the transient sources. We supply a catalog of the locations, outburst dates, peak observed luminosities, decay time estimates, and spectral properties of the transient sources, and we discuss similarities with Galactic X-ray novae. Duty cycle estimates are possible for 8 of the transients and range from 40% to 2%; upper limits to the duty cycles are estimated for an additional 15 transients and cover a similar range. We find 5 transients which have rapid decay times and may be ultra-compact X-ray binaries. Spectra of three of the transients suggest they may be faint Galactic foreground sources. If even one is a foreground source, this suggests a surface density of faint transient X-ray sources of $\gtrsim 1 \text{ deg}^{-2}$.

Subject headings: X-rays: binaries — X-rays: stars — binaries: close — galaxies: individual (M31) — accretion, accretion disks

1. Introduction

Bright X-ray transient (XRT) events provide brief glimpses into the physical state of accreting compact objects. Detailed studies of Galactic soft XRTs, also known as X-ray

¹Harvard-Smithsonian Center for Astrophysics, 60 Garden Street, Cambridge, MA 02138; williams@head-cfa.harvard.edu; garcia@head-cfa.harvard.edu

²Department of Astronomy and Astrophysics, 525 Davey Lab, Pennsylvania State University, University Park, PA 16802; bwilliams@astro.psu.edu

³Department of Physics, University College Cork, Cork, Ireland; sachi@ucc.ie; paulc@ucc.ie

⁴Institute of Space and Astronautical Science, Japan Aerospace Exploration Agency, 3-1-1 Yoshinodai, Sagamihara, Kanagawa 229-8510, Japan; naik@astro.isas.jaxa.jp

Novae (XRNe), have put constraints on the physics at work in these systems (e.g. Chen et al. 1997). Optical follow-up of 15 Galactic XRNe has revealed that the systems each contain an accreting object more massive than $\sim 3 M_{\odot}$ (McClintock & Remillard 2004), which cannot be a stable neutron star (NS). Their high X-ray luminosities ($> 10^{38} \text{erg s}^{-1}$) and millisecond X-ray variability further support the argument that these binary systems contain black holes (BHs). Therefore, these objects are among the most secure examples of black holes known (Charles 1998).

Galactic XRTs occur as both high-mass X-ray binaries (HMXBs) and low-mass X-ray binaries (LMXBs). The secondary stars of outbursting HMXBs are typically B/Be type, and the primaries are typically neutron stars (Tanaka & Shibazaki 1996). These HMXBs tend to exhibit pulsations, hard spectra, and periodically repeating outbursts.

At the same time, outbursting LMXBs have often been found to contain black hole (BH) primaries. As black holes do not have a physical surface, X-rays from the black hole X-ray novae (BHXNe) do not pulse. In addition, the spectra of BHXNe are typically softer than those of HMXBs (see the review by McClintock & Remillard 2004).

Outside the Milky Way, nearby galaxies are observed to have XRTs which are likely to be similar to those in our Galaxy. However, their greater distance makes it difficult to find optical counterparts and hinders efforts to decipher detailed information about their X-ray properties.

On the other hand, there are some advantages to extragalactic studies of XRNe. For example, in the case of M31, all of the bulge can be observed in one Chandra or XMM observation, and each such observation often reveals a new XRT source (e.g. Williams et al. 2004). These observations provide accurate positions for followup observations as well as spectral information for constraining the physical nature of the sources during these accretion events.

Because M31 is the nearest neighboring spiral galaxy, transient X-ray sources detected in M31 have been well-reported. The earliest transient source was discovered by Trinchieri & Fabbiano (1991). Many others followed, as observations of M31 by *Chandra* and *XMM-Newton* have been combed in order to catalog events that resemble Galactic XRNe.

White et al. (1995) reported a supersoft repeating transient source. Garcia et al. (2001a) reported two more new transient sources. Five additional sources were seen by Trudolyubov et al. (2001) and Osborne et al. (2001) in *XMM-Newton* and *Chandra* observations from the year 2000. Shirey (2001) reported another. Kong et al. (2002a) cataloged 10 new X-ray transients in their Chandra-ACIS study of the central region of M31. Trudolyubov et al. (2002) reported 3 more transient events from *XMM-Newton* data. Recently, Williams et al.

(2004) cataloged 8 additional transient sources from a *Chandra*-HRC survey. Finally, Di Stefano et al. (2004) have completed a survey for supersoft X-ray sources (SSS) in four regions of M31, finding 12 previously unpublished transient objects and noting 6 objects in the *ROSAT* catalog that were undetected by *Chandra* or *XMM*. Herein, we identify 2 previously-detected objects as transient candidates. All of these reports add up to 51 X-ray transients, 45 of which were detected by *XMM-Newton* or *Chandra* over a 3 year period. These 45 are presented in Table 1.

These transient sources in M31 offer the possibility of studying a statistical sample of sources all at a well-known distance (780 kpc; Williams 2003) and covering only a small part of the sky. In addition, while portions of our Galaxy cannot be effectively surveyed in low-energy X-rays due to absorption, the M31 sample does not suffer from this problem. The M31 sample allows comparative studies with the Galactic sample and adds to the number of transient sources known. Finally, M31 could harbor X-ray transient sources with uncommon properties not yet discovered in the Galaxy. Only through detailed studies of the extragalactic siblings of Galactic XRNe will be able to obtain a complete understanding of this class of X-ray sources.

In order to fully exploit the available X-ray data for M31 transients that were detected in 1999–2002, we have measured the fluxes and, where possible, the spectra of every *XMM-Newton* and *Chandra* detection of these 45 transient X-ray sources. Section 2 describes the data reduction technique for detecting and extracting the sources, measuring their fluxes and fitting their spectra. Section 3 details our results, including lightcurves, spectral parameters, and classification of the different types of spectra displayed by the transient sources. Section 4 compares the properties of these events with Galactic XRNe, and finally Section 5 summarizes our conclusions.

2. Data Reduction and Analysis

We obtained archival *Chandra* HRC and ACIS data of M31 with sampling every few months from October 1999 to August 2002. In total, 81 HRC-I observations, 23 ACIS-I observations, and 17 ACIS-S observations were included. In addition, we obtained 4 epochs of *XMM-Newton* data covering the central region of M31 and a single epoch of *XMM-Newton* data covering most of the M31 disk. Each of these *Chandra* and *XMM-Newton* observations contained at least one transient X-ray source, as well as upper-limit information for transients that appeared either before or after a given observation. The dates, instruments, observation identification (OBSID) numbers, hardness ratios, and spectral parameters for all of the *XMM-Newton* and *Chandra* ACIS observations are provided in Table 2. The HRC

observations are described in Williams et al. (2004).

2.1. Chandra Data

2.1.1. Source Detections

The ACIS data were processed using the CIAO 3.1 data analysis package with the calibration data set CALDB 2.28. We removed the effects of the ACIS-I charge transfer inefficiency using the task *acis_process_events*. We then created two images from each ACIS observation of M31. The first image was a full-resolution ($0.5''$ pixel $^{-1}$) image of an area $8.5' \times 8.5'$ centered on the aimpoint of the observation. The second image was a $4''$ pixel $^{-1}$ resolution image of the entire Chandra field. Using these two images allowed us to obtain more accurate positions and avoid blending where the Chandra PSF is very good while also allowing us to search the entire field for transient detections. We searched each of these images for sources in all of the *Chandra* ACIS data using the CIAO task *wavdetect*, which created source lists for all of the observations.

The *wavdetect* source lists that we generated and the *celldetect* source lists that were generated for each data set by the ACIS data reduction pipeline were searched for objects within $4''$ of the known transient sources, and any detections were cataloged to be used as part of the transient lightcurve. If no source was detected at the transient position, the 4σ detection limit at the transient position in the image was calculated from the exposure and background level at that location in the image. The upper-limit was converted to a luminosity using the same procedure as was used for the *XMM-Newton* upper-limits, described below (§ 2.2). Hardness ratios were calculated for each detection using background-subtracted counts (uncorrected for absorption or instrument response) in three energy bands: S (0.3–1 keV), M (1–2 keV), and H (2–7 keV). The formulas used were $HR1 = (M - S)/(M + S)$ and $HR2 = (H - S)/(H + S)$.

In addition, the source lists were searched for any bright sources that were not detected in all observations and were not in the list of published transients. By this method, two new transient sources, r1-28 and r3-8, were added to the catalog (Kong et al. 2002a). These sources have been cataloged previously in the literature, but were not considered as transient sources. Our analysis suggests that their lightcurves are comparable to most other sources previously classified as transients.

Finally, the X-ray fluxes from *Chandra*-HRC detections of the transient events were taken from Williams et al. (2004). See Williams et al. (2004) for the full details of the HRC analysis and results. Herein, we have converted each HRC flux measurement to an

unabsorbed 0.3–7 keV luminosity by assuming the spectral parameters of the most contemporaneous ACIS or *XMM-Newton* spectral fit.

2.1.2. Spectral Fits

We extracted the spectrum of each transient detection that contained enough counts ($\gtrsim 50$) using the CIAO routine *psextract*, so that each bin in the spectrum contained $\gtrsim 10$ counts (more for high-count detections). By using CIAO 3.1 to extract the spectra, the degradation of the ACIS quantum efficiency over time was taken into account in the spectral extraction. These spectra were then fit using CIAO 3.1/Sherpa (Freeman et al. 2001). Because many of our spectra contained only ~ 5 –10 data points, our goal in fitting the spectra was to find the simplest model that provided a good fit to the data. We therefore started by trying to fit a power-law, then moved on to more complex spectra as necessary.

In cases where a good fit ($\chi^2/\nu < 1.2$) could not be found using an absorbed power-law, an absorbed blackbody thermal model and an absorbed disk blackbody model were tried. If the fit was improved, we accepted the better of these two alternatives as the correct model for the source. If an acceptable fit still was not found, a neutron star atmosphere (NSA) model was tried. If the NSA model had a better overall fit or a similar fit with a more reasonable absorption correction than the other 3 models, we accepted it as the correct model for the source. The best-fitting models were then used to determine the absorption-corrected 0.3–7 keV luminosities for the lightcurves. Examples of power-law and blackbody fits are shown in Figure 1. All but a few of our final fits were acceptable ($\chi^2/\nu < 1.5$), and they provided the spectral parameters and fit statistics shown in Table 2.

In cases with high count rates, we tried adding a pileup model (Davis 2001, 2003) to the model spectrum. In these cases, we included “afterglow” events, as is the standard when applying this model. All other aspects of the fitting procedure remained the same. If the fit including pileup was an improvement according to the F -test, we included pileup in our final determination of the model spectral parameters. Source r2-67 was the only one bright enough to require a pileup model. Our fits to the 2001 August 31, 2001 October 05, 2001 November 19, and 2001 December 07 observations of r2-67 employed pileup models with pileup fractions of 0.53, 0.36, 0.27, and 0.22 respectively.

The absorption-corrected 0.3–7 keV luminosities from the spectral fits are provided in Table 2, assuming a distance of 780 kpc. If a spectral fit was performed on the source during any epoch, conversions from flux to luminosity for all low-count detections, HRC detections,

and upper-limits were performed using PIMMS version 3.4a,¹ assuming the spectral parameters from the most contemporaneous spectral fit and the effective areas as of 2003. If no spectral fit was available for the source in any epoch (s1-79, s1-82, r1-28, r2-69, r2-72, r3-46, n1-59, n1-85, and n1-88) conversions from flux to luminosity for all detections and upper-limits were performed using PIMMS, assuming a power-law spectrum with photon index 1.7, $N_H=10^{21} \text{ cm}^{-2}$, and a distance of 780 kpc.

Finally, all of the luminosities and upper-limits were combined into long-term lightcurves for each transient source. These lightcurves are shown in Figures 2–10 and discussed in § 3.2.

2.1.3. Poor Spectral Fits

There were objects with detections that contained >50 counts for which it proved difficult to obtain a reasonable spectral fit using the usual models. The SSSs were especially difficult to fit (see Di Stefano et al. 2004 for details about these sources). Therefore, the luminosities provided in Table 2 for these sources are less reliable than for the non-SSS. For example, the best fit for the SSS r2-61 had $\chi^2_\nu = 3.7$.

There was no single model type that fit every source satisfactorily. While many sources were well-fitted by an absorbed power-law model, several required other model types and/or multiple components to produce an acceptable fit. The worst case of this difficult fitting was r2-67.

Two spectra of the transient source r2-67 were studied in detail in Williams et al. (2004), and pileup was found to be important while the source was bright. We therefore included pileup in our fit to the detection of r2-67 in OBSID 1575. With 21,000 counts (0.6 ct s^{-1}), this is the highest number of counts that we have for any single *Chandra* ACIS observation of a transient source in M31, and we were therefore able to compare several different model combinations, including combining power-law with disk blackbody and power-law with single-temperature blackbody, all with absorption. After fixing the absorption column to $1.2 \times 10^{21} \text{ cm}^{-2}$, the best absorption from the *XMM-Newton* data and the January 2002 observation (ObsID 2897), a power-law fit with pileup yields a spectral index of 2.2 and $\chi^2_\nu = 10.9$ for 125 degrees of freedom (*dof*). A disk blackbody model with pileup yields an inner disk temperature of 0.62 keV and $\chi^2_\nu = 4.8$ for 125 *dof*, and a single-temperature blackbody model with pileup did not converge.

After attempting these combination models, along with single component models (no

¹<http://heasarc.gsfc.nasa.gov/docs/software/tools/pimms.html>

pileup) of all three types, we were unable to find a χ^2_ν fit better than 1.5, which is quite poor considering the large number of degrees of freedom in this data set.

The only fit better than $\chi^2_\nu = 2$ with fixed absorption was an absorbed power-law with a disk blackbody component including pileup. This model had $T_{inn} = 0.48 \pm 0.01$ keV, $\Gamma = 2.9 \pm 0.3$, and a pileup fraction of 36% ($\chi^2_\nu = 1.62$ with 122 *dof*), with a unabsorbed 0.3–7 keV luminosity of 3.2×10^{38} erg s^{−1} and 84% of the emission is from the disk blackbody component. The χ^2_ν value does not improve if absorption is a free parameter. The pileup component has a dramatic effect. The absorbed power-law with a disk blackbody component without pileup was much worse than including pileup ($\chi^2_\nu = 2.81$ with 120 *dof*). If we allow absorption to be a free parameter, the fit improves somewhat ($\chi^2_\nu = 1.84$ with 120 *dof*), but is still not as good as the fit including pileup. With the high counting rate and the obvious readout streak in this data set, pileup is clearly a concern. In addition, an *F*-test shows that there is <1% probability that pileup is not important. Therefore, we used the disk blackbody plus power-law with fixed absorption and pileup to estimate the luminosity for this detection of r2-67. The fit and residuals are shown in Figure 11.

2.2. XMM Data

Following the detection of X-ray transients in M31 with *Chandra*, we analyzed all of the publicly available *XMM-Newton* data containing the M31 disk. All isolated transient events outside of the crowded 2' X 2' region surrounding the nucleus were analyzed. The raw events were processed and filtered using the updated calibration database and analysis software package (SAS v5.4.1). The energy spectra of X-ray transients in M31 were extracted using the SAS program *xmmselect* by selecting circular regions of radius in the range of 10–15 arcsec centered at the source positions. The background spectra were extracted from the nearby source free regions. The EPIC corresponding responses and effective areas were generated by using the SAS tasks *rmfgen* and *arfgen*, respectively. The spectra were binned to a minimum of 20 counts per bin; for faint sources the spectra were binned to a minimum of 10 counts per bin. The spectral fittings were performed with the XSPEC package. Simultaneous spectral fitting was performed when spectra for more than one detector were available. The best-fit model parameters are given in Table 2.

Upper-limits were measured at the positions of transient sources detected in other observations. The 4σ detection limit at the transient position was calculated from the exposure and background level at the location where the transient had been observed in other observations. The upper-limit calculations were performed by applying the flux upper-limit to the model spectrum from the most contemporaneous spectral analysis. For sources where no

useful spectral data were available from any epoch (n1-26, n1-85, n1-88, r1-28, r2-62, r2-65, r2-66, r2-69, r2-72, r3-46, s1-27, s1-69, s1-79, s1-82, s2-62), a power-law spectrum with a photon index $\Gamma = 1.7$ and $N_H = 10^{21} \text{ cm}^{-2}$ was assumed as the typical spectrum, as determined in Shirey et al. (2001). This assumption is also reasonable considering the measured spectral properties of the transient sample (see Figure 12).

2.3. Blending

Four of our transient sources, r1-9, r1-11, r2-3, and r2-62 are within $6''$ of a known, persistent X-ray source. The *XMM-Newton* observations of these events were not reliable for determining fluxes as they were contaminated by the neighboring persistent sources. The lightcurves for these objects therefore were limited to the *Chandra* observations alone.

Source r1-9 is sandwiched between persistent sources $1''$ to its north and $2''$ to its south. The northern source is close to the M31 nucleus, but is unlikely associated with it (Garcia et al. 2001b). Di Stefano et al. (2001) have suggested that this source may be the hot stellar core of a tidally disrupted giant star.

We separated the r1-9 lightcurve from those of the neighboring sources in the HRC data by taking the lightcurve measured with a $0.7''$ box described in Williams et al. (2004). Separating the source in the ACIS data required reprocessing the event lists to remove the pixel position randomization that is part of the standard ACIS data reduction pipeline. In addition, we applied the subpixel event repositioning algorithm of Li et al. (2004) in order to obtain the best possible resolution in the nuclear region. These techniques allowed us to resolve r1-9 from the nearby sources in the ACIS observations, so that we were able to perform spectral fits on many detections and obtain upper-limits when the source was not detected.

Source r1-11 is only $3''$ away from r1-12, a bright, persistent, variable source in the central M31 bulge. Object r1-11 did not fulfill the transient criteria in the *Chandra*-HRC synoptic survey (Williams et al. 2004), possibly due to contamination from r1-12 during its weak epochs.

We remeasured the HRC lightcurve of this source with updated CIAO software, using a $3'' \times 3''$ box aperture, much smaller than the $8'' \times 8''$ box used by Williams et al. (2004), to avoid contamination from r1-12. In addition, we chose our extraction regions for the *Chandra* spectra of r1-11 so that r1-12 was not included, and we excluded observations where the two objects were not well resolved (OBSIDs 1577, 2895, 2897, and 2898) because they were too far off-axis.

This scrutiny of each data point ensures us that the lightcurve shown in Figure 3 is free from contamination. While this lightcurve clearly shows variability at about the factor of 5 level, all observations sensitive to better than 5×10^{36} erg s $^{-1}$ detect this source. While there are some non-detections in the shallower HRC data, the available data are consistent with this object being a variable source with occasional dips below $\sim 5 \times 10^{36}$ erg s $^{-1}$. This variability would not fit the Williams et al. (2004) criteria for a transient, but we include the source here as it has been classified as a transient source by Kong et al. (2002a).

Source r2-3 is only 6'' (23 pc) from r2-4, a bright variable X-ray source in the globular cluster Bol 146. The proximity to Bol 146 suggests r2-3 could be a member of the cluster. The cluster light has a full-width half-maximum of 1.2'' in the images of the Local Group Survey Massey et al. (2001), indicating a core radius of ~ 2.3 pc and placing r2-3 ~ 10 core radii from the cluster center. If r2-3 is a cluster member, it is the only transient in our catalog associated with a globular cluster. Object r2-3 did not fulfill the transient criteria in the *Chandra*-HRC synoptic survey (Williams et al. 2004), possibly due to contamination from r2-4 during its weak epochs.

We remeasured the HRC lightcurve of this source with updated CIAO software, using a 4'' X 4'' box aperture, much smaller than the 8'' X 8'' box used by Williams et al. (2004), to avoid contamination from r2-4. In addition, we chose our extraction regions for the *Chandra* spectra of r2-3 so that r2-4 was not included. Because of the separation distance, this was possible for all observations.

In contrast to r1-11, the resolved lightcurve of r2-3 appears extremely variable, with near factors of 100 changes in luminosity on timescales of months. This source may in fact be a good transient candidate; however, if it is a BHB, it has a very high duty cycle. It is brighter than 10^{36} erg s $^{-1}$ in all but 2 observations, and these observations both have upper-limits $> 10^{36}$ erg s $^{-1}$.

Source r2-62 is 5'' from the persistent, variable source r2-25 (Kong et al. 2002a). The source was only detected by the deepest *Chandra* ACIS-S observation. Since this lightcurve contained only one relevant data point (all upper-limits were above the one detected luminosity), we did not include the lightcurve for this source in Figures 2-10, nor did we attempt to estimate its properties in Table 3.

3. Results

3.1. Location

We cross-correlated our sample of transients against catalogs of globular clusters in M31 and found no clear associations. Although r2-3 could be associated with Bol 146 (see § 2.3), the $6''$ separation makes cluster membership unclear. Even so, the location of the transient sources can reveal something about their age. As discussed in Williams et al. (2004), transient events in the bulge are more likely to be black hole X-ray novae because they are likely old and therefore unlikely to be high-mass X-ray binaries. Studies of transient Galactic LMXBs show a large fraction of them to contain black holes. Therefore it is especially interesting to see the apparent clustering of transient events to the central bulge of M31.

Figure 13 shows the distribution of detected transient sources as a function of projected distance from the center of M31. Clearly most of the events lie within $10'$ (2.3 kpc) of the center of the galaxy. In fact, 30 of 45 events lie with $8'$ (1.8 kpc) of the center of the galaxy, and 39 of 45 lie within 0.5° (6.8 kpc) of the center.

Clearly some of this central concentration is due to the fact that the center of M31 has been observed far more frequently than the rest of the galaxy; however, even the unbiased *Chandra*-HRC survey of Williams et al. (2004) found half of the transient events detected occurred in the bulge. In addition, there is a clear gradient within the region of the galaxy most surveyed. With fields of view of $17' \times 17'$ and $30' \times 30'$, typical *Chandra* and XMM-*Newton* observations that are centered within $2'$ of the nucleus are unbiased out to $8'$, yet there is a clear decrease in the number of detected events with radius from the galaxy center to $8'$ away. Even though the *Chandra* PSF expands to a size of $5''$ at $8'$ off-axis, because of the low background and low source density outside of the central $2'$, the sensitivity of our typical 5 ks ACIS observation is only $\sim 10\%$ lower $8'$ off-axis than on-axis. Therefore, while there have likely been more events in the disk that have gone unobserved than events in the bulge that have gone unobserved, the events still appear to be clustered toward the galaxy center.

As the M31 bulge contains little or no recent star formation, these X-ray binaries are most likely old ($\gtrsim 1$ Gyr). Therefore most of them are likely LMXBs. Since a high percentage of Galactic LMXBs that produce bright X-ray novae contain dynamically confirmed black hole primaries, the locations of these events suggest that they arise primarily from BH-containing X-ray binaries.

3.2. Lightcurves

The lightcurves for all of the transient sources detected in at least one observation are shown in Figures 2–10, including all observations during the relevant time period made by *XMM-Newton*, *Chandra* ACIS and *Chandra* HRC. To limit confusion, if there were 2 or more upper-limits measured within one week, only the faintest upper-limit is plotted in the figure. All upper-limits brighter than the brightest detection were removed.

Some lightcurves have observations that appear very close in time but yield different luminosity measurements. The long time line can be deceiving in this regard as these observations are separated by at least several days. These sources can change in luminosity by factors of 10 or more in that time span. For example, in the lightcurve of r1-5 the first three HRC detections appear to be significantly brighter than the early ACIS detections. Unfortunately, since none of the observations were simultaneous and the HRC yields no spectral information, we can only conclude that the source was either brighter or had a different spectrum during those HRC observations. In cases where the observations truly were within a day or two of simultaneous (see Table 2 for dates), the luminosities from different instruments are consistent within the errors.

Those sources without any bright detections (n1-26, r1-35, r2-61, s1-27, s1-69) could not be classified using the available data. Sources r2-66 and s2-62 were not detected in any single epoch observation. We therefore did not include lightcurves for these sources at all, as they were only detected by stacking images from multiple epochs in Di Stefano et al. (2004). Source r2-62 was only detected in the deepest ACIS-S observation, and there were no upper-limits for this source that showed it was fainter than this luminosity. We therefore did not include the lightcurve for r2-62 either. These eight sources do not fit the criteria for an X-ray transient used in Williams et al. (2004), but were classified as such by the criteria of Di Stefano et al. (2004).

We fit an exponential decay to each lightcurve assuming the brightest detection as the lightcurve peak and assuming half of the upper-limit flux (and an error equal to half of the upper-limit) for HRC (1σ) upper-limits, and one third of the upper-limit flux (and an error equal to one third of the upper-limit) for ACIS and XMM (4σ) upper-limits. This method was reasonable because the ACIS and XMM upper-limits were more conservative than those taken from the much shallower HRC data. The fit was terminated when there were 2 non-detections in succession. Such exponential decay is representative of the overall shape of the lightcurves of most Galactic X-ray novae (Chen et al. 1997). Lightcurves for sources with no bright detections (n1-26, r1-35, r2-66, s2-62) or a decay curve with fewer than 3 data points between luminosity peaks (n1-26, n1-86) could not provide a reliable estimate of e -folding time. In some cases (n1-89, r2-60, r2-61, s1-27, s1-69) there was only a single non-detection

after the brightest detection. For these two-point decay curves, if the upper-limit was at least a factor of e fainter than the detection, the decay time was constrained to less than the time between the two observations.

These e -folding decay time estimates help to characterize the length of the burst, but they are only estimates based on our coarsely sampled lightcurves. We note that the time separation of the data points can be three or four months in many cases. In addition, the lightcurves may not have decayed exponentially in all cases (Shahbaz et al. 1998; Williams et al. 2005a). For these reasons, the decay time measurements should only be considered rough approximations.

We counted the distinct outbursts in the lightcurve of each source that showed such distinct outbursts. For example, r2-67 clearly shows only one outburst during the studied time period. Source r2-8 shows 2 outbursts clearly separated by several months of non-detections. This number, given in Table 3, helps to show the burst frequency of the sources. The majority (23) of the XRTs showed only 1 clear outburst. Seven sources showed 2 outbursts, and 3 sources showed 4 outbursts. The remaining 9 XRTs detected in single epochs were either too faint (e.g. n1-26 and r1-35) or had lightcurves that were too complex (e.g. r1-23 and r2-3) to clearly count outbursts.

The date and unabsorbed (0.3–7 keV) luminosity of the brightest detection, the number of lightcurve points used in the fit, the faintest upper-limit, the bright/faint luminosity ratio, the best-fit e -folding decay time, the number of distinct outbursts observed, the duty cycle estimate, and the lightcurve type for each transient source are provided in Table 3. In addition, a histogram of the number of transients as a function of e -folding time is given in Figure 14, showing a peak at ~ 25 days for the non-SSSs.

A similar peak was seen for Galactic outbursts (Chen et al. 1997). For comparison, we fit our distribution with a Gaussian using least-squares. The best fit, shown with the dotted line in Figure 14, has a $\langle \log(\tau_d) \rangle = 1.5 \pm 0.5$. This value is consistent with the Galactic distribution of $\langle \log(\tau_d) \rangle = 1.24 \pm 0.36$. The SSSs and QSSs have longer decay times, but these lightcurves are the most poorly constrained, with large correction factors for their luminosity estimates and peak detections only a factor of a few brighter than the upper-limits of the non-detections.

Figure 15 shows the decay time estimates, maximum observed luminosities, and duty cycle estimates of the XRTs as a function of their projected distance from the galaxy center. No clear correlation is found in the XRT properties with their position in the galaxy. The only noteworthy feature in the figures is the three faintest XRTs are all SSSs (plotted with filled circles), hinting that these sources may not be appropriate members of the XRT sample.

On the other hand, three of the SSSs are indistinguishable from the rest of the sample in both plots, indicating that they are appropriate members of the sample.

A plot of the decay time vs. the peak luminosity of the transient events is provided in Figure 16. No correlation is apparent, which adds confidence that there are no strong biases in the data or analysis that would cause more luminous bursts to appear to have shorter decays. This figure also shows that the ~ 30 day peak in Figure 14 contains sources covering 2 decades of peak luminosity. We note that our brightest luminosity transient, n1-86, is not shown. No decay time was measured for this source because its brightest detection was in the final observation.

In addition, one identifier of accreting BHs is a luminosity $> L_{edd}$ for a typical ($1.4 M_{\odot}$) NS. Figure 15 shows a histogram of the peak observed luminosities of the M31 transients. Our sample contains 4 events brighter than $2.5 \times 10^{38} \text{ erg s}^{-1}$, which fit this criterion.

In addition, the range of peak luminosities (see Figure 14) is similar to the Galactic sample (Chen et al. 1997), considering the different sampling rates and number of years of monitoring. Their sample contains 33 sources, ours has 30 with measured decay times, not including SSSs or QSSs. Their sample has 12 events with peak luminosities $> 10^{38} \text{ erg s}^{-1}$; ours has 7. Their sample has 3 events with peak luminosities $> 10^{39} \text{ erg s}^{-1}$; ours has 1. This source, n1-86, is very soft and has a large absorption correction. Furthermore, the effective temperature of the spectral fit indicates that n1-86 may be a foreground source (see § 3.7). If so, its luminosity would be only $\sim 10^{35} \text{ erg s}^{-1}$.

The lower number of bright peak luminosities may be due to the sampling of our data and the length of our timeline. Since our lightcurves are only sampled at about once per 2 months, we are not likely to have measured these transients at their absolute highest luminosities, considering Galactic transients only stay at their peak brightness for \sim days (Chen et al. 1997; McClintock & Remillard 2004). In any case, the Chen et al. (1997) sample covers 26 years (1970–1996) of observations, while our sample only covers 3 years (1999–2002). If the rate of $10^{39} \text{ erg s}^{-1}$ XRNe is $\sim 0.1 \text{ yr}^{-1}$, we should not expect to see more than 1 in 3 years of monitoring M31.

3.3. Duty Cycles

The outburst numbers were used to estimate the duty cycles for XRTs with measured decay times and peak/quiescent luminosity ratios > 15 . These estimates are also provided in Table 3. The duty cycles for sources showing evidence for only a single outburst are given as upper-limits, assuming that no outbursts were missed during the course of the observations

shown in the lightcurve. It is certainly possible that this assumption is incorrect for a few of the more poorly sampled objects, but since most sources appear to be faint more often than they are bright, we believe it more likely that they were faint for significantly more time before and after our sampling period than that we missed an outburst during the sampling period. Therefore this assumption is more conservative than alternative assumptions (e.g. that this measurement is a good estimate of the real duty cycle or that this measurement is a lower limit to the real duty cycle).

A histogram of the cumulative number of XRTs as a function of duty cycle is shown in Figure 17. About half of the measured duty cycles are <0.1 , and all but three are <0.2 . This distribution is compatible with the Galactic sample of Chen et al. (1997), which shows recurrence times ranging from months to ~ 100 years, with most recurrence times >1 year. If one assumes the decay time of ~ 20 days, this large range of recurrence times yields a wide range in duty cycles from 0.0005–0.3, with most duty cycles <0.1 .

The lightcurves reveal a wide variety of photometric behavior, but they can be described as falling into four categories. Category one contains sources like r1-11, which are active during most epochs but disappear occasionally. We classify these as “High Duty Cycle” (HDC) transients. Category two contains sources like r2-8, which appear for a few months more than once over the course of the studied time period. We classify these as “Medium Duty Cycle” (MDC) transients. Category three contains sources like r1-5, which only appear once but take years to disappear. We classify these as “Long Decay” (LD) transients. Finally, category four contains sources like r3-126, which appear only once for a short time, sometimes so short that they are only detected in one observation. We classify these as “Low Duty Cycle” (LDC) transients. The classification of each source is provided in Table 3. For a some sources (n1-26, r1-35, r2-61, r2-65, s1-18, s1-27, s1-69) we could not reliably determine which class they fell into, and no classification is reported in Table 3.

3.4. Short Term Variability

We tested our sources for short-term variability (type I bursts) through Kolmogorov-Smirnov (KS) tests of the arrival times of the photons against a constant arrival time distribution. We applied this test to the ACIS detection of each source with the highest number of counts, if that detection contained over 100 counts. All of these tests yielded P values greater than 0.75, providing no evidence for significant short-term variability in any of the transient events.

We tested the sensitivity of the KS test by creating monte carlo photon arrival time

distributions for detections containing 100 counts distributed over 5 ks, the typical length of our ACIS observations. We ran such tests for bursts of 10, 100 and 1000 s. These tests showed that our observations were more sensitive to longer bursts. They were sensitive to factor of 2.3 changes in flux that lasted 1000 s, factor of 10 changes in flux that lasted 100 s, and factor of 100 changes in flux that lasted 10 s at the 50% confidence level. Galactic X-ray Type I bursts (see Fig. 3.1 in review by Lewin et al. 1993) typically last ~ 10 –100 s with factors of ~ 10 –20 changes in flux, so that we would be sensitive only to the brightest and longest bursts. For example, our data would not be sensitive to the Type I bursts in Aql X-1 (Czerny et al. 1987), because its flux increased by a factor of 10 for less than 100 s.

3.5. Periodic Outbursts

We inspected the lightcurves for transients that may be periodic. Only 3 sources in the sample showed more than 2 distinct outbursts.

Sources r1-11 and r2-16 appear to have undergone ~ 4 outbursts from 1999 to 2002. The outbursts appear at regular intervals, suggesting that these transient sources have outburst periods of ~ 0.7 yr and decay time estimates of 40 and 90 days, respectively. These numbers are comparable to the values of the Galactic neutron star LMXB transient Aql X-1, which undergoes a 30–60 day outburst every ~ 200 days (Šimon 2002). These sources also have some detections with the hardest spectra in the sample, with photon indexes as low as 0.8 (r1-11) and 0.5 (r2-16), but they are not expected to be HMXBs because they are $< 1.3'$ from the center of M31 where there is no known young stellar population (e.g. Stephens et al. 2003). The absorption columns for the sources are consistent with $\sim 10^{21}$ cm $^{-2}$, so that the secondary is not likely heavily extincted. If these sources are HMXBs, they have secondaries fainter than $M_V \sim -1$ (see § 4.1). In any case, the recurrence and spectral properties hint that these transients may have neutron star primaries.

Source r3-8 also showed 4 outbursts, but this source is much softer than r2-16 and r1-11. Source r3-8 has equivalent hardness ratios to several SSSs and therefore is unlikely to be an HMXB.

3.6. Spectral Properties

The results of the photometric and spectroscopic measurements of all of the transient source detections are given in Table 2. Histograms of the measured photon indexes (Γ) and absorption columns are shown in Figure 12. Again, a wide range of spectral properties

are seen, from hard spectra like those of s1-1 and r1-5, which are well-fit by power-law models with $\Gamma \sim 1.5$, to very soft spectra like those of r3-8 and n1-86, which have hardness comparable to those of SSSs.

There is also a wide range of absorption column values for these sources, ranging from 4×10^{20} to 10^{22} cm². The errors on the absorption measurements tend to be larger than those on the Γ measurements, reflecting the effective area of the telescopes at low energies. Nevertheless, most of the measured absorption values for these sources are 0.4×10^{21} – 3×10^{21} cm², typical absorption values for M31 X-ray sources, suggesting that the vast majority of these measurements are reliable.

Generally, the spectra of the sources appear to vary between observations, as evidenced by the hardness ratios. In many cases, the errors on the spectral parameters are too large to reliably quantify the spectral changes. On the other hand, there are some cases where the changes are large enough to be statistically significant in the parameters of the spectral fits, such as r2-3, whose photon index varies between 1.6 ± 0.2 to 2.7 ± 0.2 , and r3-16 whose index varies from 1.4 ± 0.2 to 2.0 ± 0.2 . Absorption values also can also be variable in these transient sources, indicating that they are self-absorbed. For example, the absorption toward r1-5 varies between $0.7 \pm 0.2 \times 10^{21}$ cm² and $2.9 \pm 0.8 \times 10^{21}$ cm², and the absorption toward r2-8 varies between $0.3 \pm 0.3 \times 10^{21}$ cm² and $2.2^{+1.1}_{-0.8} \times 10^{21}$ cm².

3.7. Neutron Star Atmosphere Fits

Some of the softest transients were best-fitted by a neutron star atmosphere (NSA) spectral model (Zavlin et al. 1996). This model provides the spectra emitted from the hydrogen atmosphere of a neutron star. When fitting this model, we fixed the magnetic field to zero, the radius to 10 km, and the mass to $1.4 M_{\odot}$, allowing only the effective temperature of the atmosphere to be fitted. Three sources were well-fitted by this model (n1-86, r3-8, and s1-18); however, the fluxes supplied by all of the NSA fits indicate (assuming $L_X = 4\pi R^2 \sigma T_{eff}^4$) that the emitting source has a radius of $\sim 10^5$ km if located in M31, making them much larger than neutron stars and even larger than white dwarf stars. If they are neutron stars (10 km radius), they have $L_X \sim 10^{29}$ – 10^{30} erg s^{−1} and are at a distance of < 100 pc, making them Galactic foreground sources. The local space density of these sources implied by this result is not consistent with Galactic observations. However, if these sources are cataclysmic variables (CVs), their space density is consistent with the local value.

Source n1-86 is only well-fitted ($\chi^2/\nu < 1.5$) in all observations with a NSA model; however, a blackbody model provides an equally good fit for the January 2002 ACIS detection.

Because the NSA fits required a slightly lower absorption correction and provided the only acceptable fits to the January 2002 *XMM* detection and February 2002 ACIS detection, we took NSA as the appropriate model for all detections of this source. The effective temperature and luminosity (assuming the source is in M31) that come out of this fit implies that the radius of the star is $>10^5$ km. Since this radius is even large for a white dwarf, it is possible that the source is a Galactic foreground neutron star or CV. This possibility would also explain the high luminosity measured for this source (2×10^{39} erg s $^{-1}$). If n1-86 is in M31, it had the highest X-ray luminosity of any transient yet observed in M31. If it is a foreground neutron star or CV, its luminosity was $<10^{36}$ erg s $^{-1}$.

Source s1-18 only has a single detection useful for spectral fitting. The small number of counts is well-fitted by both a blackbody model ($\chi^2/\nu = 1.3$) and a NSA model ($\chi^2/\nu = 0.6$). Because the NSA fit is better, we took it as the correct model. In any case, the absorption-corrected luminosity did not depend significantly on the choice of model for this source. The effective temperature and luminosity that come out of this fit implies a large radius of $>10^4$ km, indicating that the source may be in the Galactic foreground with luminosity $<10^{36}$ erg s $^{-1}$.

The most significant improvement for a spectral fit using the NSA model was for r3-8. All of the high-count *XMM* and *Chandra* detections of this source were well-fitted with the NSA model. In addition, the detection with the highest number of counts, from *XMM* in January 2002, could only be fitted with the NSA model. No other model, including composite models, fit the source with $\chi^2/\nu < 2$. The NSA model fits the spectrum quite well, as shown in Figure 18. Although quantitatively the fit has $\chi^2/\nu = 1.3$, it clearly follows the continuum correctly, and no other single-component model has such a shape to its spectrum, showing the observed peak at ~ 0.5 keV and a sharp drop to higher energies. The fact that only this model fits the spectrum suggests that r3-8 is a compact star with an atmosphere effective temperature of 2×10^5 K. Assuming the source is in M31 provides a luminosity indicating that the radius of the star is $>10^5$ km. Again, this result suggests the source is in the Galactic foreground with a luminosity of $<10^{36}$ erg s $^{-1}$.

Because these sources appear to be in the Galactic foreground, we investigated whether such a number of faint foreground transient sources in our sample is reasonable and what sort of objects could be the sources of this X-ray emission. It is possible that such a number of faint foreground transients has gone undetected until now. A surface density of such transient sources, with fluxes of $\sim 10^{-13}$ – 10^{-12} erg cm $^{-2}$ s $^{-1}$, of $\gtrsim 1$ per square degree would not contradict the results of Galactic surveys such as, for example, the ChaMPlane survey (Grindlay et al. 2003), even though ChaMPlane does not repeat observations many times and therefore would not be sensitive to such transient sources.

Even though the only single-component spectral model that fits these data is a NSA model, these sources are not likely to be neutron stars. With the measured temperatures, neutron stars would have luminosities of $\sim 10^{29} - 10^{30}$ erg s $^{-1}$. Our survey was only sensitive to such sources within ~ 200 pc, yielding a volume density of $\gtrsim 10^{-3}$ pc $^{-3}$ for these sources. Such a volume density is unreasonable under the assumption that CVs (whose space density is of order 10^{-5} pc $^{-3}$; Grindlay et al. 2005) are more common than transient neutron stars.

The sources are too bright to be CVs with spherically symmetric emission. The measured temperatures yield spherically symmetric luminosities of $\gtrsim 10^{35}$ erg s $^{-1}$ for white dwarf radii. At these luminosities, the distances are $\gtrsim 10$ kpc, putting the sources far out of the Galactic disk. These luminosities and locations are both atypical of CVs.

The most reasonable explanation for these sources is that they are foreground polars. In this case, the radii of the primary stars is ~ 8000 km (Warner 1995), and the fractional emitting surface area is $\sim 10^{-3}$ (Mauche 1999), making the luminosities of the sources $\sim 10^{32} - 10^{33}$ erg s $^{-1}$ (3×10^{32} erg s $^{-1}$ for n1-86; 7×10^{32} erg s $^{-1}$ for r3-8; 2×10^{32} erg s $^{-1}$ for s1-18), and their distances less than a few kpc (300 pc for n1-86; 1 kpc for r3-8; 2 kpc for s1-18). These temperatures, luminosities and distances would be reasonable for polars (see Warner 1995 and Cropper 1990 reviews). Furthermore, with these distances and luminosities, the space density of the sources would be $\gtrsim 4 \times 10^{-7}$ pc $^{-3}$, which is similar to several published values for the space density of polars (Cropper 1990; Warner 1995).

It is unusual that the spectra of these sources are well-fit by an NSA model if they are not neutron stars, but we note that the NSA model was simply the only single-component model with which we could fit the data. It is possible that multi-component models with more free parameters, such as those used to fit the spectra of polars, could also fit these data. There are similarities between the spectra of our NSA sources and those of known polars. For example, these sources are all very soft, and some polars are known to have strong soft emission (Ramsay et al. 2005a). Furthermore, although typical XMM spectra of polars in the bright phase have spectra that are flat or decreasing from 0.2–1 keV (see figures in Ramsay et al. 2001, 2004), spectra similar to that observed for r3-8 do exist (e.g., RX J1914+24; Ramsay et al. 2005b).

Many polars have spectra that are difficult to fit and require modeling with multi-component blackbody spectra. Our XMM spectrum of r3-8 provided enough counts to attempt a fit with such multi-component models. An absorbed ($N_H = 2.3 \times 10^{21}$ cm $^{-2}$) blackbody spectrum with $kT = 71$ eV plus a broad Gaussian emission line at 0.52 keV, similar to the best-fit model of the polar RX J1914+24 (Ramsay et al. 2005b), provides a good fit with $\chi^2/\nu = 124.5/98$. We therefore suggest, based on the space density and spectra, that these sources are Galactic foreground polars and that the spectra of polars can

mimic those of NSAs. More observations of these very soft transient sources are needed to confirm this possibility.

3.8. Hardness-Luminosity and Color-Color Diagrams

To monitor the spectral properties of the transient events, we produced hardness-luminosity (hardness-intensity proxy) diagrams from the hardness ratio HR2 and absorption-corrected 0.3–7 keV luminosities from the ACIS-I and ACIS-S detections of the transient events. These diagrams were only generated for events with at least 3 total ACIS detections. This requirement limited the number of diagrams to 18, all of which are shown in Figures 19 and 20. We have plotted the ACIS-S and ACIS-I ratios with different symbols because the ratios are calculated from straight counts. Because ACIS-S is more sensitive to soft photons than ACIS-I, the ACIS-S ratios will be systematically softer than those from ACIS-I for the same source.

These diagrams show a wide range of behavior. For example, r1-9, r1-35, r2-63, and r3-8 exhibit very soft ratios at all luminosities, providing only upper-limits to their hardness ratio in many cases. This behavior clearly sets them apart as SSSs. In addition, the diagrams of some sources, such as r1-5, r1-23, r2-3, r2-8, r2-16, r2-67, and r3-16, show interesting patterns.

The diagram for r1-5 reveals a range of luminosities with a hard spectrum with a hint of a transition from the bright, hard state to a soft state at similar luminosity. Note that the ACIS-S ratios are softer because of the higher sensitivity to soft photons. Source r1-23 appears to vary between a low-soft and high-hard state. Source r2-3 reveals a range of hardness ratios that is consistent with a transition from a low-soft state to a high-hard state, with a single data point suggesting an extension to a low-hard state. The bimodal HR diagram looks similar to that for Galactic Z-sources, suggesting we are seeing the Normal Branch and Flaring Branch but missing the Horizontal Branch (see Figure 3.1 of Kuulkers 1995). The diagram for r2-16 shows an almost circular pattern, going from a low-soft state, to a low-hard state, to a high-hard state, to a high-soft state. This pattern is also seen in some Galactic Z-sources, such as Cyg X-2, (see Figure 4.3 of Kuulkers 1995).

At the same time, there are several similarities with Galactic black hole binaries. For example, r2-3 and r2-8 show transitions from a high-hard state to a low-soft state. Source r2-67 appears to show the same kind of transition, although we note that some of this effect could be due to pileup during the high luminosity observations hardening the spectrum. The pattern is reminiscent of the most luminous portions of the diagram for XTE J1859+226

and GRO 1655-40, which show their softest colors at intermediate fluxes (Done & Gierliński 2003). This comparison makes sense because we only detect the M31 transients when they are bright. Source r3-16 has very large errors in hardness ratio at low luminosities, but it appears to undergo a similar transition near its peak luminosity. In addition, the hardness luminosity diagram for r1-19 shows a slightly softer color at $2\text{--}4 \times 10^{36}$ erg s^{−1} than at brighter and fainter luminosities, and that of r2-16 shows a strong dip in hardness at $\sim 10^{37}$ erg s^{−1}. This behavior appears comparable to that of XTE J1550-564 from $\sim 0.001\text{--}0.005$ L_{Edd} (see Fig.2 of Done & Gierliński 2003). Several sources appear soft when they are brightest, such as r2-28 and r2-29, also similar to many Galactic black holes.

We also created color-color diagrams of these sources, shown in Figures 21 and 22. When these types of diagrams are made for bright Galactic LMXBs, they tend to fall into two categories: “Z” sources and atoll sources (Hasinger & van der Klis 1989). The color-color diagrams for “Z” sources form the shape of a “Z” as they evolve from hard to soft and back to hard; the others form “atolls”, where they jump more quickly from hard to soft and back. The color-color diagrams of several of sources that are not supersoft (r1-9, r1-35, r2-63, r3-8 are SSSs) resemble “Z” sources, such as r1-5, r1-11, r1-23, r2-3, r2-8, and r2-16. For example, the color-color and hardness-intensity diagrams for r2-16 resemble those of Cyg X-2 in the Normal Branch and Flaring Branch (Kuulkers 1995), but this linear track from soft to hard colors is also seen in black hole binaries (Done & Gierliński 2003), making it difficult to distinguish between the two possibilities. Source r3-16 has a distinctive color-color diagram that appears to follow a linear track at hard colors but then breaks up at soft colors, similar to tracks seen in the color-color diagrams of some Galactic black holes, such as XTE J1550-564.

4. Discussion

4.1. Galactic Comparisons

Transient X-ray sources have been studied in detail in the Galaxy. Therefore comparisons between the general spectral and photometric properties of the Galactic and M31 populations may aid in drawing conclusions about the types of X-ray binaries causing the outbursts observed in M31. In addition, any differences between the M31 outbursts and those observed in the Galaxy will raise new questions about the M31 X-ray binary population. It has already been suggested that the LMXB population in the M31 bulge contains roughly the same BH/NS ratio as that seen in the Galaxy (Williams et al. 2004). Now we would like to discover if the M31 XRTs themselves share similar physical properties to their Galactic siblings. Bright X-ray transient events originate from several different types

of objects. These include supersoft sources (SSSs), high-mass X-ray binaries (HMXBs), and low-mass X-ray binaries (LMXBs).

The physical nature of SSSs is not well-understood, but they are straight-forward to identify, as their outbursts are relatively faint ($\lesssim 10^{37}$ erg s $^{-1}$), and their X-ray spectral properties are supersoft, with $\Gamma \gtrsim 3.5$ or blackbody temperatures of ~ 100 eV. SSSs are often seen as recurrent X-ray transients (e.g. White et al. 1995). The most widely accepted model for SSSs consists of a white dwarf accreting from a companion at a high enough rate ($\gtrsim 10^{-7} M_{\odot} \text{yr}^{-1}$) to sustain stable nuclear burning (van den Heuvel et al. 1992; Rappaport et al. 1994). However, the definition of the class is broad enough that NS binaries and isolated stellar core models have been considered (Greiner et al. 1991; Di Stefano et al. 2001).

There are several sources in our catalog that could be SSSs. Sources n1-26, r1-9, r1-35, r2-60, r2-61, r2-62, r2-63, r2-65, r2-66, r3-115, s1-18, s1-27, s1-69, and s2-62 are already classified as QSSs and SSSs (Di Stefano et al. 2001, 2004). In addition, r3-128 has a spectrum that is not well fit by any model, but the best fit is a very low temperature (0.04 keV) thermal model, suggesting it may be supersoft. Finally, r3-8 and n1-86 have hardness ratios consistent with typical SSSs and their spectra are equally difficult to fit, only providing good χ^2 values for a low-temperature NSA model.

HMXB transient X-ray events typically occur near star forming regions, as they contain high-mass donor stars. These donor stars are typically Be stars (Tanaka & Shibazaki 1996). These stars have spectral types between O8.5 and B2 (Negueruela 1998) and optical magnitudes of $-4.8 \lesssim M_V \lesssim -2.4$ (Cox 2000). The X-ray spectra of these outbursts tend to be harder than the other types of XRTs, with photon indexes near 1. In addition, these systems tend to have periodic repeating outbursts thought to occur during close encounters between the high-mass donor star and the neutron star primary (Tanaka & Shibazaki 1996). Two of our sources have outbursts that appear to be periodic, r1-11 and r2-16. These two sources are the most likely HMXBs in the bulge. However, inspection of the 2004 January 23 *HST* ACS observation described in Williams et al. (2005b), reveals no bright stars ($B \lesssim 23.5$; $M_V \lesssim -1$) within an arcsec of the X-ray positions of r1-11 or r2-16. Only r3-16 and r3-115 have bright, persistent optical counterparts (Williams et al. 2004; Di Stefano et al. 2004). Finally the XRT spectra are nearly all soft, so that very few of the sources in our catalog are likely to be HMXBs. Outside the bulge, n1-87 and s1-1 have spectral properties that are consistent with a HMXBs; however, we note that several sources outside the bulge do not have spectral data available.

Neutron star LMXBs that undergo bright (10^{38} erg s $^{-1}$), long (decay time >10 day) X-ray outbursts are rare, possibly due to the presence of a hard stellar surface (e.g. King et al. 1997; King & Kolb 1997). Only a handful of such transient X-ray sources are known

(McClintock & Remillard 2004). Examples of such systems are Aql X-1 (Koyama et al. 1981) and Cen X-4 (Matsuoka et al. 1980), which were shown to contain neutron stars by the presence of type I X-ray bursts in their lightcurves. In addition to their type I bursts, these XRTs have longer outbursts that recur on timescales of years, mimicking the bursts of BHBs because they have X-ray luminosities of up to $\sim 2 \times 10^{38}$ erg s $^{-1}$ and decay times of about 1 month. Although our data are not sufficient to reliably determine how many sources in our catalog may be neutron star LMXB systems, the small number of known neutron star XRNe in our Galaxy suggests that there are at most only a handful. Furthermore, our short-term variability tests were sensitive to the bright-end of type I bursts (factor of ~ 10 flux increases with ~ 100 s duration; see § 3.4), and no short-term variability was detected in our sample.

Some neutron star LMXBs are in ultra-compact X-ray binaries (UCXBs), which tend to form in areas of high stellar density, such as the cores of globular clusters or near the centers of galaxies. A population of these sources has been observed in the Galactic center (e.g. Heise et al. 1999; King 2000). These sources are believed to have neutron star primaries. Their X-ray spectra are typical of LMXBs containing neutron star primaries, power-law with $\Gamma \sim 1.7$. Their short orbital periods ($\lesssim 2$ hr) show that they are close binary systems. The small orbital separation restricts the size of the accretion disk, resulting in short outburst decay times and faint outbursts. These systems have decay times of only < 1 week, and peak luminosities of $\lesssim 10^{37}$ erg s $^{-1}$. Their rapid variations occur on the time scale of a few days, as in 4U 1820-30 (Šimon 2003). In addition, they can undergo “superbursts” with luminosities of $> 10^{38}$ erg s $^{-1}$, as in 4U 1820-30, but the decay time is < 1 day (Strohmayer & Brown 2002). Four sources (r2-61, r3-43, r3-128, and s1-69) were detected only once, allowing the possibility of such a short decay time. In addition, there are five sources (n1-59, n1-85, r2-65, r2-69, and r3-8) that were detected once, then were not detected in the following observation but reappeared two or three observations later for a single observation. Three of these 9 sources (r2-61, r2-65, and s1-69) have previously been classified SSSs by others (Di Stefano et al. 2004), and one source (r3-8) may be a foreground CV (see § 3.7). Therefore, five sources have the potential to be UCXBs. Of these five, the most likely are r2-69, r3-43, and r3-128 because they are located in the high stellar density M31 bulge.

Succinctly, many soft Galactic XRT events have BH primaries. These XRTs share many properties with the few neutron star LMXB transient events described above, including long recurrence timescales, outburst decay timescales of ~ 1 month, and X-ray luminosities. However, there are some differences, including softer X-ray spectra, with $\Gamma > 1.7$ and/or temperatures of $\lesssim 1$ keV. Although their outbursts can be as faint as 10^{36} erg s $^{-1}$, some of these systems have outbursts $> 2 \times 10^{38}$ erg s $^{-1}$, ruling out neutron star progenitors. Radial velocity studies of Galactic XRT sources with these properties suggests $\sim 90\%$ of them are

BHBs (McClintock & Remillard 2004). It is therefore likely that most of the sources in our catalog, excluding the SSSs, are BHBs.

5. Conclusions

We have put together all of the *Chandra* and *XMM-Newton* data sets pertaining to 45 transient X-ray sources in M31 detected from October 1999 to August 2002. These data have provided a catalog of positions, spectral properties, and lightcurves for transient X-ray sources in M31.

The locations of these transient sources indicate that they most often form near the center of the galaxy, suggesting that most of them are old LMXBs. The distribution of peak luminosities of these sources range from $\sim 10^{36}$ to $\sim 10^{39}$ erg s $^{-1}$, similar to Galactic XRTs. The estimated e -folding decay times are similar to those seen in Galactic XRNe, also suggesting that many of these sources are BH-containing LMXBs.

The transient source lightcurves and positions indicate 5 potential UCXBs, 3 of which are located in the M31 bulge. Two other sources have possible periodic outbursts and hard spectra consistent with HMXBs, but they have no optical counterparts brighter than $M_V \approx -1$.

The lightcurves also constrain the transient rate in M31. If we take only those sources with the best lightcurves (Hi/Lo >15, measured decay time, and one at least one clear outburst), there were 26 transient sources seen in the 35 months covered by our sample. Removing the total of ~ 9 months during which M31 was not observable during this time period yields a transient rate in M31 of ~ 1 per month, consistent with the previous result in Williams et al. (2004). The rate of X-ray novae in the Galaxy (~ 2.6 per year; Chen et al. 1997), hinting that the rate in M31 could be higher. However, since the Galactic rate is likely incomplete because sampling the entire Galaxy is much more difficult than sampling M31, the similarity of the two rates is noteworthy.

Furthermore, these data are some of the best available for studying the duty cycles of a large sample of transient sources. We have used the lightcurves to constrain the duty cycles of the transients, finding about half have duty cycles < 0.1 and all but 3 sources have duty cycles < 0.2 . This range is similar to that seen in the Galaxy (Chen et al. 1997), where the transients have duty cycles ranging from 0.0005–0.3 and most duty cycles are < 0.1 .

The spectra of the sources provided more details about their physical properties. Some source spectra are well-fitted by simple absorbed power-law models with photon indexes

ranging from 1–4 and absorption values from $0.1\text{--}10 \times 10^{21} \text{ cm}^{-2}$. Others are only well-fitted by multi-component spectral models, including power-law plus blackbody or disk blackbody models with temperatures 0.03–1.2 keV. Still other source spectra are too soft to provide an acceptable fit with any of these model combinations. Three soft sources are well-fit by a neutron-star atmosphere model, but the best-fit effective temperatures indicate that these sources must be in the Galactic foreground. The surface density of these sources ($\gtrsim 1 \text{ deg}^{-2}$) is consistent with that of magnetic CVs (polars) but higher than expected for neutron stars, suggesting that these sources are foreground polars. Their spectra are also well-fit by multi-component models similar to those of some polars, showing that polar spectra and neutron star atmosphere spectra can be similar.

Clearly the discovery of these XRTs marks only the beginning of their study. These sources provide the largest extra-galactic sample of XRTs available in one galaxy and will open the door to future comparison studies of outbursting X-ray binary populations in galaxies.

We thank Robin Barnard for suggesting the NSA model for fitting the spectra of some of the soft sources. Support for this work was provided by NASA through grant GO-9087 from the Space Telescope Science Institute and through grant GO-3103X from the *Chandra* X-Ray Center.

REFERENCES

- Charles, P. 1998, in *Theory of Black Hole Accretion Disks*, 1
- Chen, W., Shrader, C. R., & Livio, M. 1997, *ApJ*, 491, 312
- Cox, A. N. 2000, *Allen’s astrophysical quantities* (*Allen’s astrophysical quantities*, 4th ed. Publisher: New York: AIP Press; Springer, 2000. Edited by Arthur N. Cox. ISBN: 0387987460)
- Cropper, M. 1990, *Space Science Reviews*, 54, 195
- Czerny, M., Czerny, B., & Grindlay, J. E. 1987, *ApJ*, 312, 122
- Davis, J. E. 2001, *ApJ*, 562, 575
- Davis, J. E. 2003, “Talk at the HEAD 2002 meeting”, <http://space.mit.edu/CXC/analysis/davis/head2002/>
- Di Stefano, R., Greiner, J., Murray, S., & Garcia, M. 2001, *ApJ*, 551, L37

- Di Stefano, R., et al. 2004, *ApJ*, 610, 247
- Done, C., & Gierliński, M. 2003, *MNRAS*, 342, 1041
- Freeman, P., Doe, S., & Siemiginowska, A. 2001, in *Proc. SPIE Vol. 4477*, p. 76-87, *Astronomical Data Analysis*, Jean-Luc Starck; Fionn D. Murtagh; Eds., 76
- Garcia, M., Kong, A., Primini, F., McClintock, J., Murray, S., & Di Stefano, R. 2001a, *The Astronomer’s Telegram*, 79, 1
- Garcia, M. R., Kong, A., Primini, F. A., Barmby, P., Di Stefano, R., McClintock, J. E., & Murray, S. S. 2001b, in *Two Years of Science with Chandra*, Abstracts from the Symposium held in Washington, DC, 5-7 September, 2001.
- Greiner, J., Hasinger, G., & Kahabka, P. 1991, *A&A*, 246, L17
- Grindlay, J., et al. 2003, *Astronomische Nachrichten*, 324, 57
- Grindlay, J. E., et al. 2005, *ArXiv Astrophysics e-prints*
- Hasinger, G., & van der Klis, M. 1989, *A&A*, 225, 79
- Heise, J., in’t Zand, M. J. J., Smith, S. M. J., Muller, M. J., Ubertini, P., Bazzano, A., Cocchi, M., & Natalucci, L. 1999, *Astrophysical Letters Communications*, 38, 297
- King, A. R. 2000, *MNRAS*, 315, L33
- King, A. R., & Kolb, U. 1997, *ApJ*, 481, 918
- King, A. R., Kolb, U., & Szuszkiewicz, E. 1997, *ApJ*, 488, 89
- Kong, A., Garcia, M., Murray, S., Primini, F., McClintock, J., & Di Stefano, R. 2001, *The Astronomer’s Telegram*, 76, 1
- Kong, A. K. H., Garcia, M. R., Primini, F. A., Murray, S. S., Di Stefano, R., & McClintock, J. E. 2002a, *ApJ*, 577, 738
- Kong, A. K. H., Garcia, M. R., Primini, F. A., Murray, S. S., & McClintock, J. E. 2002b, *The Astronomer’s Telegram*, 97, 1
- Koyama, K., et al. 1981, *ApJ*, 247, L27
- Kuulkers, E. 1995, *Ph.D. Thesis*
- Lewin, W. H. G., van Paradijs, J., & Taam, R. E. 1993, *Space Science Reviews*, 62, 223

- Li, J., Kastner, J. H., Prigozhin, G. Y., Schulz, N. S., Feigelson, E. D., & Getman, K. V. 2004, *ApJ*, 610, 1204
- Massey, P., Hodge, P. W., Holmes, S., Jacoby, G., King, N. L., Olsen, K., Saha, A., & Smith, C. 2001, in *American Astronomical Society Meeting*, Vol. 199, 13005
- Matsuoka, M., et al. 1980, *ApJ*, 240, L137
- Mauche, C. W. 1999, in *ASP Conf. Ser. 157: Annapolis Workshop on Magnetic Cataclysmic Variables*, 157
- McClintock, J. E., & Remillard, R. A. 2004, in *Compact Stellar X-ray Sources* (astro-ph/0306213)
- Negueruela, I. 1998, *A&A*, 338, 505
- Osborne, J. P., et al. 2001, *A&A*, 378, 800
- Ramsay, G., Cropper, M., Córdova, F., Mason, K., Much, R., Pandel, D., & Shirey, R. 2001, *MNRAS*, 326, L27
- Ramsay, G., Cropper, M., Mason, K. O., Córdova, F. A., & Friedhorsky, W. 2004, *MNRAS*, 347, 95
- Ramsay, G., Hakala, P., Marsh, T., Nelemans, G., Steeghs, D., & Cropper, M. 2005a, *A&A*, 440, 675
- Ramsay, G., Hakala, P., Wu, K., Cropper, M., Mason, K. O., Córdova, F. A., & Friedhorsky, W. 2005b, *MNRAS*, 357, 49
- Rappaport, S., Di Stefano, R., & Smith, J. D. 1994, *ApJ*, 426, 692
- Shahbaz, T., Charles, P. A., & King, A. R. 1998, *MNRAS*, 301, 382
- Shirey, R. 2001, *IAU Circ.*, 7659, 1
- Shirey, R., et al. 2001, *A&A*, 365, L195
- Stephens, A. W., et al. 2003, *AJ*, 125, 2473
- Strohmayer, T. E., & Brown, E. F. 2002, *ApJ*, 566, 1045
- Tanaka, Y., & Shibazaki, N. 1996, *ARA&A*, 34, 607
- Trinchieri, G., & Fabbiano, G. 1991, *ApJ*, 382, 82

- Trudolyubov, S., Priedhorsky, W., Borozdin, K., Mason, K., & Cordova, F. 2002, IAU Circ., 7798, 2
- Trudolyubov, S. P., Borozdin, K. N., & Priedhorsky, W. C. 2001, ApJ, 563, L119
- Šimon, V. 2002, A&A, 381, 151
- Šimon, V. 2003, A&A, 405, 199
- van den Heuvel, E. P. J., Bhattacharya, D., Nomoto, K., & Rappaport, S. A. 1992, A&A, 262, 97
- Warner, B. 1995, Cataclysmic variable stars (Cambridge Astrophysics Series, Cambridge, New York: Cambridge University Press, —c1995)
- White, N. E., Giommi, P., Heise, J., Angelini, L., & Fantasia, S. 1995, ApJ, 445, L125
- Williams, B. F. 2003, AJ, 126, 1312
- Williams, B. F., Garcia, M. R., Kong, A. K. H., Primini, F. A., King, A. R., Di Stefano, R., & Murray, S. S. 2004, ApJ, 609, 735
- Williams, B. F., Garcia, M. R., Kong, A. K. H., Primini, F. A., & Murray, S. S. 2005a, ApJ, 620, 723
- Williams, B. F., Garcia, M. R., Primini, F. A., McClintock, J. E., & Murray, S. S. 2005b, ApJ, accepted
- Zavlin, V. E., Pavlov, G. G., & Shibano, Y. A. 1996, A&A, 315, 141

Table 1. Transient Catalog

Source	RA (J2000)	DEC (J2000)	Detection References
n1-26	0 46 39.0	41 39 07.5	Di Stefano et al. 2004
n1-59	0 45 45.76	41 50 30.1	Williams et al. 2004
n1-85	0 45 28.05	41 54 10.9	Williams et al. 2004
n1-86	0 44 14.0	41 22 04	Trudolyubov et al. 2002
n1-87	0 44 15.9	41 30 58	Trudolyubov et al. 2002
n1-88	0 44 28.4	41 56 28.1	Garcia et al. 2001a
n1-89	0 44 38.1	41 45 11	Trudolyubov et al. 2002
r1-5	0 42 42.16	41 16 08.42	Trudolyubov et al. 2001/Kong et al. 2002a
r1-9	0 42 44.3	41 16 07.6	Kong et al. 2002a
r1-11	0 42 43.88	41 16 30.0	Kong et al. 2002a
r1-19	0 42 46.00	41 16 19.8	Kong et al. 2002a
r1-23	00 42 43.9	41 16 04.0	Kong et al. 2002a
r1-28	0 42 43.79	41 15 14.5	new
r1-34	0 42 39.58	41 16 14.6	Trinchieri & Fabbiano 1991/Garcia et al. 2001a
r1-35	0 42 43.0	41 16 03.9	Di Stefano et al. 2004
r2-3	0 43 03.24	41 15 28.0	Kong et al. 2002a
r2-8	0 42 56.89	41 18 44.0	Kong et al. 2002a/Osborne et al. 2001
r2-16	0 42 45.22	41 17 22.5	Kong et al. 2002a
r2-28	0 42 34.75	41 15 23.3	Kong et al. 2002a
r2-29	0 42 34.43	41 18 09.6	Trudolyubov et al. 2001
r2-60	0 42 43.9	41 17 55.5	Di Stefano et al. 2004
r2-61	0 42 47.3	41 15 07.2	Di Stefano et al. 2004
r2-62	0 42 39.2	41 14 24.4	Di Stefano et al. 2004
r2-63	0 42 59.3	41 16 42.8	Di Stefano et al. 2004
r2-65	0 42 47.0	41 14 12.4	Di Stefano et al. 2004
r2-66	0 42 49.0	41 19 47.1	Di Stefano et al. 2004
r2-67	0 43 05.66	41 17 03.3	Williams et al. 2004/Kong et al. 2001
r2-69	0 42 42.16	41 14 24.4	Williams et al. 2004
r2-72	0 42 51.2	41 16 39.8	Garcia et al. 2001a
r3-8	0 43 18.8	41 20 16.5	new
r3-16	0 43 09.87	41 19 01.2	Kong et al. 2002a/Kong et al. 2002b
r3-43	0 42 21.0	41 18 08.5	Kong et al. 2002a
r3-46	0 42 17.06	41 15 08.8	Kong et al. 2002a
r3-115	0 43 07.14	41 18 09.5	Williams et al. 2004/Di Stefano et al. 2004
r3-125	0 42 05.71	41 13 29.7	Osborne et al. 2001

Table 1—Continued

Source	RA (J2000)	DEC (J2000)	Detection References
r3-126	0 43 19.52	41 17 56.7	Osborne et al. 2001/Trudolyubov et al. 2001
r3-128	0 43 08.5	41 18 20	Shirey 2001
s1-1	0 42 34.97	40 57 21.5	Williams et al. 2004
s1-18	0 41 49.2	40 56 43.8	Di Stefano et al. 2004
s1-27	0 41 39.9	41 04 25.7	Di Stefano et al. 2004
s1-69	0 41 41.9	41 07 16.7	Di Stefano et al. 2004
s1-79	0 40 55.16	40 56 03.5	Williams et al. 2004
s1-80	0 41 54.63	40 56 47.4	Williams et al. 2004/Kong et al. 2002b
s1-82	0 42 20.82	40 51 36.3	Williams et al. 2004
s2-62	0 38 38.7	40 15 11.3	Di Stefano et al. 2004

Table 2. Spectral Fits to Transient Detections

Source	Date	Inst	OBSID	Counts ^a	Model ^b	N _H ^c	Γ ^d	kTorlog(T) ^e	χ ² /ν	Q ^f	HR-1 ^g	HR-2 ^h	L _X ⁱ
n1-26	08-Mar-2001	ACIS-S	2053	7	0.33±0.43	-0.35±0.62	0.5±0.2
n1-26	03-Jul-2001	ACIS-S	2054	21	-0.35±0.32	-1.12±0.73	1.1±0.4
n1-59	26-Jan-2002	XMM	0109270301	90/ ... / ...	pl	0.1 ^{+1.1} _{-0.1}	1.8 ^{+1.2} _{-0.4}	...	16.61/21	0.734	-0.22±0.23	-0.63±0.41	1.1 ^{+0.9} _{-0.2}
n1-86	05-Jan-2002	XMM	0109270701	... /318/208	nsa	2.9 ^{+0.7} _{-0.4}	...	5.140 ^{+0.030} _{-0.050}	28.94/29	0.468	-1.01±0.09	-0.98±0.12	677.0±445.0
n1-86	08-Jan-2002	ACIS-I	2897	129	nsa	2.8±0.5	...	5.141±0.026	9.28/10	0.506	-1.03±0.16	-1.15±0.18	623.4±65.5
n1-86	06-Feb-2002	ACIS-I	2896	84	nsa	3.9±1.8	...	5.219±0.058	8.65/6	0.194	-0.97±0.19	-0.75±0.16	2018.4±246.6
n1-87	05-Jan-2002	XMM	0109270701	418/129/ ...	pl	10.5 ^{+3.1} _{-2.1}	1.2 ^{+0.2} _{-0.2}	...	40.97/36	0.262	0.84±0.14	0.94±0.08	10.5±2.3
n1-89	05-Jan-2002	XMM	0109270701	462/127/99	pl	1.1 ^{+0.3} _{-0.3}	2.0 ^{+0.1} _{-0.1}	...	52.53/57	0.643	0.01±0.08	-0.34±0.1	7.9±0.6
n1-89	26-Jan-2002	XMM	0109270301	... /76/ ...	pl	0.2 ^{+1.3} _{-0.2}	2.0 ^{+0.4} _{-0.4}	...	21.32/21	0.440	-0.07±0.22	-0.2±0.28	4.6 ^{+3.4} _{-0.9}
r1-5	13-Oct-1999	ACIS-I	303	1055	pl	2.0±0.3	1.5±0.1	...	59.70/47	0.101	0.46±0.04	0.37±0.04	83.1±2.6
r1-5	11-Dec-1999	ACIS-I	305	245	pl	0.9±0.7	1.3±0.3	...	18.48/19	0.491	0.39±0.09	0.38±0.09	76.2±4.9
r1-5	27-Dec-1999	ACIS-I	306	269	pl	1.0±0.6	1.4±0.2	...	32.74/21	0.049	0.39±0.08	0.25±0.09	63.7±3.9
r1-5	29-Jan-2000	ACIS-I	307	320	pl	2.9±0.8	1.7±0.2	...	29.34/26	0.296	0.56±0.08	0.45±0.08	75.8±4.3
r1-5	16-Feb-2000	ACIS-I	308	391	pl	2.0±0.6	1.6±0.2	...	32.31/32	0.452	0.39±0.07	0.39±0.07	81.5±4.1
r1-5	01-Jun-2000	ACIS-S	309	568	pl	0.9±0.2	1.2±0.1	...	19.90/23	0.648	0.17±0.05	0.09±0.05	68.3±2.9
r1-5	02-Jul-2000	ACIS-S	310	565	pl	0.7±0.2	1.2±0.1	...	31.16/22	0.093	0.12±0.05	0.02±0.05	62.6±2.7
r1-5	29-Jul-2000	ACIS-I	311	359	pl	2.1±0.7	1.6±0.2	...	26.84/28	0.527	0.53±0.08	0.46±0.08	65.6±3.5
r1-5	27-Aug-2000	ACIS-I	312	274	pl	1.7±0.8	1.6±0.2	...	12.90/21	0.912	0.45±0.08	0.35±0.09	51.4±3.1
r1-5	13-Dec-2000	ACIS-I	1581	193	pl	1.4±1.0	1.3±0.2	...	9.40/14	0.804	0.53±0.11	0.47±0.11	45.7±3.3
r1-5	13-Jan-2001	ACIS-S	1854	298	pl	0.9±0.4	1.3±0.2	...	15.27/24	0.913	0.14±0.07	0.03±0.08	37.2±2.2
r1-5	18-Feb-2001	ACIS-I	1582	129	pl	2.3±1.3	1.7±0.3	...	9.38/9	0.403	0.53±0.13	0.46±0.14	26.7±2.4
r1-9	13-Oct-1999	ACIS-I	303	114	pl	2.6±1.1	4.2±0.7	...	11.89/10	0.293	-0.16±0.09	-0.85±0.15	34.9±3.6
r1-9	11-Dec-1999	ACIS-I	305	21	-0.33±0.20	-1.00±0.33	20.4±5.0
r1-9	29-Jan-2000	ACIS-I	307	7	-0.33±0.43	-1.00±0.71	8.3±3.6
r1-9	16-Feb-2000	ACIS-I	308	57	pl	3.6±1.4	4.1±0.7	...	3.05/6	0.803	0.08±0.11	-0.76±0.19	89.2±12.5
r1-9	01-Jun-2000	ACIS-S	309	244	pl	2.6±0.7	3.4±0.5	...	31.94/27	0.234	-0.18±0.06	-0.79±0.09	70.2±5.2

Table 2—Continued

Source	Date	Inst	OBSID	Counts ^a	Model ^b	N _H ^c	Γ^d	kTorlog(T) ^e	χ^2/ν	Q ^f	HR-1 ^g	HR-2 ^h	L _X ⁱ
r1-9	02-Jul-2000	ACIS-S	310	74	pl	1.5±0.7	3.8±0.8	...	20.37/7	0.005	-0.70±0.12	-0.93±0.15	13.5±1.8
r1-9	29-Jul-2000	ACIS-I	311	35	0.25±0.15	-0.79±0.29	16.4±3.2
r1-9	27-Aug-2000	ACIS-I	312	28	-0.06±0.14	-0.86±0.25	15.0±3.3
r1-9	10-Jun-2001	ACIS-I	1583	9	-0.23±0.28	-1.00±0.50	4.1±1.5
r1-9	05-Oct-2001	ACIS-S	1575	877	pl	1.9±0.3	3.6±0.2	...	50.73/38	0.081	-0.34±0.03	-0.84±0.05	29.8±1.1
r1-9	11-Aug-2002	ACIS-I	4360	36	0.23±0.12	-0.77±0.22	17.3±2.9
r1-11	13-Oct-1999	ACIS-I	303	145	pl	2.4±1.2	1.8±0.4	...	7.60/10	0.668	0.48±0.11	0.21±0.13	12.3±1.0
r1-11	11-Dec-1999	ACIS-I	305	80	pl	1.1±2.2	0.8±0.6	...	2.88/4	0.578	0.63±0.17	0.57±0.18	23.6±3.6
r1-11	27-Dec-1999	ACIS-I	306	68	pl	3.0±3.0	1.5±0.8	...	5.20/3	0.158	0.69±0.18	0.55±0.21	16.9±2.5
r1-11	29-Jan-2000	ACIS-I	307	51	pl	0.7±1.6	2.0±0.6	...	1.34/2	0.512	0.28±0.17	-0.04±0.19	9.2±1.0
r1-11	16-Feb-2000	ACIS-I	308	61	pl	0.4±0.8	1.5±0.0	...	0.64/2	0.726	0.25±0.17	0.27±0.17	10.0±1.3
r1-11	01-Jun-2000	ACIS-S	309	81	pl	0.4±0.8	1.4±0.7	...	6.87/4	0.143	-0.09±0.12	-0.38±0.15	8.2±0.6
r1-11	02-Jul-2000	ACIS-S	310	21	-0.24±0.25	-0.58±0.32	2.9±0.7
r1-11	29-Jul-2000	ACIS-I	311	45	0.50±0.19	0.11±0.23	8.5±1.3
r1-11	13-Dec-2000	ACIS-I	1581	58	pl	3.4±3.5	1.6±0.8	...	0.11/2	0.949	0.63±0.21	0.61±0.21	14.9±1.8
r1-11	13-Jan-2001	ACIS-S	1854	96	pl	0.9±0.8	1.6±0.5	...	12.05/6	0.061	-0.06±0.12	-0.11±0.13	10.2±1.2
r1-11	18-Feb-2001	ACIS-I	1582	36	0.37±0.25	0.46±0.24	7.8±1.4
r1-11	10-Jun-2001	ACIS-I	1583	71	pl	3.5±2.8	2.0±0.8	...	1.29/3	0.732	0.64±0.18	0.53±0.19	16.0±1.9
r1-11	05-Oct-2001	ACIS-S	1575	216	pl	2.4±0.6	2.1±0.2	...	16.87/18	0.532	0.24±0.08	-0.22±0.10	3.6±0.1
r1-11	19-Nov-2001	ACIS-I	1585	101	pl	4.2±3.0	2.2±0.7	...	1.27/3	0.737	0.60±0.18	0.42±0.20	18.6±2.2
r1-11	06-Feb-2002	ACIS-I	2896	81	pl	2.7±2.0	2.0±0.4	...	4.50/5	0.480	0.39±0.15	0.24±0.16	17.4±2.0
r1-11	11-Aug-2002	ACIS-I	4360	34	0.67±0.25	0.47±0.29	12.2±2.1
r1-19	13-Oct-1999	ACIS-I	303	35	-0.17±0.19	-0.20±0.20	3.0±0.6
r1-19	11-Dec-1999	ACIS-I	305	10	0.16±0.39	0.02±0.42	2.3±0.8
r1-19	29-Jan-2000	ACIS-I	307	9	0.41±0.35	-1.04±0.87	2.0±0.7
r1-19	29-Jul-2000	ACIS-I	311	43	0.45±0.20	0.11±0.23	9.0±1.4

Table 2—Continued

Source	Date	Inst	OBSID	Counts ^a	Model ^b	N _H ^c	Γ^d	kTorlog(T) ^e	χ^2/ν	Q ^f	HR-1 ^g	HR-2 ^h	L _X ⁱ
r1-19	13-Dec-2000	ACIS-I	1581	8	0.00±0.32	0.23±0.29	1.8±0.7
r1-19	13-Jan-2001	ACIS-S	1854	73	pl	1.4±1.0	2.1±0.6	...	4.68/4	0.321	-0.02±0.13	-0.41±0.17	8.3±1.0
r1-19	10-Jun-2001	ACIS-I	1583	14	-0.09±0.31	-0.33±0.35	2.6±0.7
r1-19	31-Aug-2001	ACIS-I	1577	22	0.10±0.23	-0.21±0.27	4.7±1.1
r1-19	05-Oct-2001	ACIS-S	1575	245	pl	1.1±0.4	2.3±0.3	...	31.45/21	0.066	-0.22±0.07	-0.47±0.08	3.4±0.2
r1-19	19-Nov-2001	ACIS-I	1585	40	0.52±0.19	0.00±0.24	8.7±1.4
r1-19	07-Dec-2001	ACIS-I	2895	14	0.29±0.28	-0.25±0.38	3.0±0.9
r1-19	02-Jun-2002	ACIS-I	2898	8	0.72±0.47	0.00±1.00	1.8±0.7
r1-19	11-Aug-2002	ACIS-I	4360	17	0.43±0.29	0.00±0.36	3.4±0.9
r1-23	13-Oct-1999	ACIS-I	303	58	pl	0.4±2.0	1.4±0.7	...	1.73/3	0.631	0.19±0.16	0.02±0.17	3.9±0.5
r1-23	11-Dec-1999	ACIS-I	305	20	0.07±0.25	-0.33±0.31	4.2±1.0
r1-23	27-Dec-1999	ACIS-I	306	9	0.20±0.32	-0.33±0.43	1.8±0.7
r1-23	29-Jan-2000	ACIS-I	307	16	0.29±0.28	-0.25±0.37	3.4±0.9
r1-23	16-Feb-2000	ACIS-I	308	27	0.09±0.21	-0.46±0.29	5.8±1.2
r1-23	01-Jun-2000	ACIS-S	309	43	-0.15±0.16	-0.58±0.22	16.8±2.7
r1-23	02-Jul-2000	ACIS-S	310	42	-0.02±0.17	-0.46±0.22	16.5±2.7
r1-23	29-Jul-2000	ACIS-I	311	30	0.85±0.31	0.77±0.37	19.3±3.7
r1-23	27-Aug-2000	ACIS-I	312	32	0.37±0.23	0.19±0.25	21.9±4.0
r1-23	13-Dec-2000	ACIS-I	1581	12	0.46±0.33	0.00±0.41	8.6±2.7
r1-23	13-Jan-2001	ACIS-S	1854	60	pl	2.8±1.9	3.7±1.2	...	1.12/2	0.571	-0.17±0.15	-0.31±0.16	16.8±2.3
r1-23	18-Feb-2001	ACIS-I	1582	15	-0.23±0.29	-0.33±0.31	11.0±3.0
r1-23	05-Oct-2001	ACIS-S	1575	171	pl	1.4±0.5	2.4±0.3	...	10.88/15	0.761	-0.04±0.08	-0.45±0.10	2.9±0.3
r1-23	19-Nov-2001	ACIS-I	1585	14	0.29±0.32	0.22±0.33	3.3±0.9
r1-23	07-Dec-2001	ACIS-I	2895	37	0.41±0.21	0.31±0.22	8.9±1.5
r1-23	06-Feb-2002	ACIS-I	2896	24	0.36±0.24	-0.25±0.33	5.5±1.2
r1-23	11-Aug-2002	ACIS-I	4360	24	0.38±0.25	-0.09±0.31	5.3±1.1

Table 2—Continued

Source	Date	Inst	OBSID	Counts ^a	Model ^b	N _H ^c	Γ^d	kTorlog(T) ^e	χ^2/ν	Q ^f	HR-1 ^g	HR-2 ^h	L _X ⁱ
r1-28	11-Dec-1999	ACIS-I	305	4	0.51±0.57	0.01±0.72	0.9±0.5
r1-28	29-Jan-2000	ACIS-I	307	9	-0.20±0.46	0.15±0.39	4.5±1.6
r1-28	11-Aug-2002	ACIS-I	4360	19	0.00±0.27	-0.08±0.28	3.7±0.9
r1-34	05-Oct-2001	ACIS-S	1575	3033	pl	1.7±0.1	1.8±0.1	...	117.39/109	0.275	0.19±0.02	-0.09±0.02	50.1±0.9
r1-34	19-Nov-2001	ACIS-I	1585	138	pl	3.9±1.8	2.7±0.5	...	2.58/9	0.979	0.55±0.11	0.19±0.13	45.6±3.9
r1-35	01-Jun-2000	ACIS-S	309	17	-0.64±0.38	-1.01±0.50	1.3±0.3
r1-35	02-Jul-2000	ACIS-S	310	19	-1.01±0.52	-0.77±0.43	1.4±0.4
r1-35	13-Jan-2001	ACIS-S	1854	14	-1.05±0.76	-1.10±0.80	1.1±0.3
r1-35	05-Oct-2001	ACIS-S	1575	129	pb	0.7±0.3	3.4±0.3	0.018±0.002	5.04/4	0.283	-0.78±0.15	-1.00±0.17	3.1±0.3
r2-3	13-Oct-1999	ACIS-I	303	481	pl	3.1±0.6	2.7±0.2	...	16.33/19	0.635	0.33±0.05	-0.14±0.07	62.6±2.9
r2-3	11-Dec-1999	ACIS-I	305	6	0.02±0.52	0.02±0.51	1.4±0.6
r2-3	27-Dec-1999	ACIS-I	306	166	pl	1.4±0.7	2.2±0.3	...	11.19/13	0.595	0.27±0.09	-0.07±0.11	32.9±2.6
r2-3	29-Jan-2000	ACIS-I	307	129	pl	2.2±1.0	2.4±0.4	...	9.14/10	0.519	0.33±0.10	-0.11±0.13	31.1±2.7
r2-3	16-Feb-2000	ACIS-I	308	194	pl	1.4±0.9	1.9±0.3	...	13.05/14	0.522	0.42±0.09	0.06±0.11	38.2±2.7
r2-3	01-Jun-2000	ACIS-S	309	325	pl	1.5±0.4	1.9±0.2	...	18.75/25	0.809	0.05±0.06	-0.33±0.08	35.0±2.0
r2-3	02-Jul-2000	ACIS-S	310	311	pl	2.0±0.4	2.0±0.2	...	19.06/25	0.794	0.12±0.06	-0.25±0.08	48.8±2.8
r2-3	29-Jul-2000	ACIS-I	311	314	pl	0.7±0.6	1.6±0.2	...	17.35/24	0.833	0.33±0.07	0.17±0.08	46.9±2.7
r2-3	13-Dec-2000	ACIS-I	1581	69	pl	1.1±1.7	2.3±0.8	...	0.47/3	0.925	0.24±0.15	-0.08±0.17	22.8±2.8
r2-3	13-Jan-2001	ACIS-S	1854	68	pl	1.4±0.9	2.8±0.6	...	2.93/4	0.569	-0.18±0.13	-0.73±0.20	10.4±1.3
r2-3	18-Feb-2001	ACIS-I	1582	106	pl	3.8±2.4	2.1±0.9	...	1.51/6	0.959	0.59±0.13	0.26±0.16	33.6±3.3
r2-3	10-Jun-2001	ACIS-I	1583	88	pl	1.5±1.4	2.2±0.6	...	4.56/6	0.601	0.18±0.12	-0.25±0.14	19.9±2.1
r2-3	31-Aug-2001	ACIS-I	1577	216	pl	2.3±1.1	2.1±0.3	...	10.33/16	0.849	0.46±0.09	0.18±0.10	44.4±3.0
r2-3	05-Oct-2001	ACIS-S	1575	3085	pl	1.7±0.1	2.0±0.1	...	114.90/112	0.407	0.14±0.02	-0.23±0.03	53.8±0.9
r2-3	19-Nov-2001	ACIS-I	1585	260	pl	1.0±0.7	1.5±0.2	...	22.21/24	0.567	0.45±0.08	0.33±0.08	55.1±3.4
r2-3	07-Dec-2001	ACIS-I	2895	64	pl	0.4±1.7	1.8±0.6	...	0.81/3	0.848	0.31±0.15	0.09±0.17	25.9±3.3
r2-3	08-Jan-2002	ACIS-I	2897	196	pl	2.8±0.9	2.5±0.3	...	20.09/15	0.169	0.43±0.09	0.09±0.11	46.8±3.4

Table 2—Continued

Source	Date	Inst	OBSID	Counts ^a	Model ^b	N _H ^c	Γ^d	kTorlog(T) ^e	χ^2/ν	Q ^f	HR-1 ^g	HR-2 ^h	L _X ⁱ
r2-3	06-Feb-2002	ACIS-I	2896	293	pl	2.2±0.8	2.0±0.2	...	14.20/22	0.894	0.50±0.08	0.29±0.09	56.6±3.3
r2-3	02-Jun-2002	ACIS-I	2898	156	pl	0.4±0.7	1.8±0.3	...	9.27/12	0.680	0.24±0.10	0.03±0.11	24.5±2.0
r2-3	11-Aug-2002	ACIS-I	4360	170	pl	2.7±1.2	2.3±0.4	...	10.54/13	0.649	0.55±0.10	0.20±0.12	39.8±3.1
r2-8	13-Dec-2000	ACIS-I	1581	66	pl	0.4±2.3	1.7±1.2	...	5.83/3	0.120	0.28±0.15	0.03±0.17	11.6±1.4
r2-8	27-Dec-2000	XMM	0112570601	173/ ... / ...	pl	0.9 ^{+1.5} _{-0.9}	1.9 ^{+0.9} _{-0.6}	...	18.94/19	0.461	-0.23±0.12	-0.33±0.13	8.3 ^{+5.9} _{-8.3}
r2-8	13-Oct-1999	ACIS-I	303	370	pl	1.5±0.6	1.5±0.2	...	26.68/30	0.640	0.48±0.07	0.37±0.08	25.5±1.3
r2-8	27-Aug-2000	ACIS-I	312	45	0.17±0.17	-0.24±0.21	8.5±1.3
r2-8	05-Oct-2001	ACIS-S	1575	30	0.41±0.28	0.19±0.32	0.5±0.1
r2-16	11-Dec-1999	ACIS-I	305	58	pl	0.4±1.4	1.7±0.6	...	4.41/3	0.221	-0.09±0.15	-0.17±0.16	10.5±1.4
r2-16	27-Dec-1999	ACIS-I	306	39	0.43±0.21	0.16±0.23	7.8±1.3
r2-16	29-Jan-2000	ACIS-I	307	74	pl	0.6±1.9	1.1±0.6	...	6.58/3	0.087	0.67±0.19	0.64±0.19	14.9±1.7
r2-16	16-Feb-2000	ACIS-I	308	29	0.77±0.27	0.45±0.36	7.4±1.4
r2-16	10-Jun-2001	ACIS-I	1583	60	pl	0.4±2.8	0.5±0.4	...	0.32/2	0.854	0.54±0.19	0.49±0.20	29.2±3.8
r2-16	29-Jun-2001	XMM	0109270101	1554/570/595	pl	1.1 ^{+0.1} _{-0.1}	1.8 ^{+0.0} _{-0.1}	...	140.14/154	0.781	-0.1±0.05	-0.24±0.05	15.7±0.6
r2-16	05-Oct-2001	ACIS-S	1575	97	pl	1.7±0.9	2.2±0.4	...	11.18/7	0.131	0.17±0.11	-0.40±0.16	1.5±0.2
r2-16	06-Jan-2002	XMM	0112570101	1319/313/322	pl	1.2 ^{+0.2} _{-0.2}	2.4 ^{+0.1} _{-0.1}	...	181.5/130	0.002	-0.4±0.04	-0.62±0.05	8.8±0.5
r2-16	08-Jan-2002	ACIS-I	2897	94	pl	0.9±1.2	1.8±0.3	...	4.32/8	0.827	0.38±0.12	0.22±0.13	23.0±2.6
r2-16	06-Feb-2002	ACIS-I	2896	90	pl	0.4±1.8	1.2±0.6	...	2.37/5	0.795	0.39±0.14	0.34±0.15	19.4±2.1
r2-28	27-Dec-1999	ACIS-I	306	62	pl	0.4±1.2	1.9±0.5	...	1.62/3	0.655	0.32±0.15	-0.17±0.19	10.1±1.3
r2-28	29-Jan-2000	ACIS-I	307	71	pl	0.5±1.1	2.8±0.6	...	3.56/4	0.469	0.05±0.12	-0.77±0.21	13.4±1.6
r2-28	16-Feb-2000	ACIS-I	308	20	0.13±0.25	-0.27±0.32	4.9±1.1
r2-29	25-Jun-2000	XMM	0112570401	1922/872/691	pl	0.9 ^{+0.1} _{-0.1}	2.3 ^{+0.1} _{-0.1}	...	182/164	0.160	-0.29±0.04	-0.56±0.04	29.9±0.8
r2-29	02-Jul-2000	ACIS-S	310	50	pl	0.4±1.9	2.0±0.6	...	2.49/2	0.288	0.19±0.16	-0.26±0.20	15.1±2.1
r2-29	29-Jul-2000	ACIS-I	311	27	0.28±0.24	0.02±0.27	4.7±0.9
r2-29	27-Aug-2000	ACIS-I	312	16	0.37±0.37	0.44±0.36	2.9±0.7
r2-60	13-Jan-2001	ACIS-S	1854	8	-1.01±0.72	-1.02±0.73	89.6±33.2

Table 2—Continued

Source	Date	Inst	OBSID	Counts ^a	Model ^b	N _H ^c	Γ ^d	kTorlog(T) ^e	χ ² /ν	Q ^f	HR-1 ^g	HR-2 ^h	L _X ⁱ
r2-60	29-Jun-2001	XMM	0109270101	459/ ... / ...	pb	2.3 ^{+0.1} _{-0.1}	4.3 ^{+0.2} _{-0.2}	0.016 ^{+0.003} _{-0.003}	74.52/72	0.396	-0.68±0.08	-0.93±0.09	260.0 ^{+170.0} _{-110.0}
r2-60	05-Oct-2001	ACIS-S	1575	132	bb	2.4±0.3	...	0.018±0.002	12.15/8	0.145	-1.01±0.17	-1.01±0.17	451.6±41.0
r2-60	06-Jan-2002	XMM	0112570101	204/ ... / ...	pb	2.6 ^{+0.3} _{-0.2}	4.2 ^{+0.4} _{-0.4}	0.015 ^{+0.000} _{-0.000}	64.66/53	0.131	-0.76±0.2	-1±0.22	40.1 ^{+4.5} _{-4.3}
r2-61	05-Oct-2001	ACIS-S	1575	97	bb	0.4±0.2	...	0.035±0.005	18.73/5	0.002	-0.79±0.25	-0.98±0.29	1.0±0.1
r2-62	05-Oct-2001	ACIS-S	1575	22	0.13±0.23	-0.92±0.50	0.4±0.1
r2-63	01-Jun-2000	ACIS-S	309	12	-1.04±0.80	-1.02±0.78	6.6±2.0
r2-63	02-Jul-2000	ACIS-S	310	6	-1.01±0.55	-1.00±0.55	3.4±1.4
r2-63	13-Jan-2001	ACIS-S	1854	9	5.4±1.9
r2-63	29-Jun-2001	XMM	0109270101	84/ ... / ...	bb	1	...	0.022 ^{+0.001} _{-0.002}	17.138/19	0.581	-0.62±0.52	-0.69±0.56	9.4 ^{+12.0} _{-4.9}
r2-63	05-Oct-2001	ACIS-S	1575	132	bb	1.1±0.4	...	0.023±0.004	3.14/6	0.791	-0.96±0.21	-0.98±0.22	14.9±1.4
r2-63	06-Jan-2002	XMM	0112570101	162/20/28	pb	1.5 ^{+0.1} _{-0.1}	1.4 ^{+1.2} _{-0.5}	0.022 ^{+0.007} _{-0.004}	104.16/80	0.036	-0.55±0.25	-0.98±0.31	29.0±1.4
r2-65	13-Jan-2001	ACIS-S	1854	13	-1.11±0.68	-0.61±0.47	1.9±0.6
r2-65	05-Oct-2001	ACIS-S	1575	22	-1.11±0.37	-0.99±0.33	0.4±0.1
r2-67	31-Aug-2001	ACIS-I	1577	1276	dbb	1.2±0.1	...	0.506±0.036	57.14/57	0.470	0.44±0.04	0.50±0.04	296.0±8.3
r2-67	05-Oct-2001	ACIS-S	1575	21000	dbb	1.2±0.1	...	0.479±0.013	197.29/122	0.000	0.09±0.01	-0.46±0.01	315.5±2.2
r2-67	19-Nov-2001	ACIS-I	1585	892	dbb	1.2±0.1	...	0.471±0.048	51.63/33	0.021	0.37±0.04	0.12±0.05	204.6±7.2
r2-67	07-Dec-2001	ACIS-I	2895	663	dbb	1.2±0.1	...	0.474±0.067	40.04/30	0.104	0.33±0.05	-0.02±0.05	128.0±5.0
r2-67	06-Jan-2002	XMM	0112570101	8746/2365/2563	pl	1.25 ^{+0.05} _{-0.05}	3.1 ^{+0.1} _{-0.0}	...	579.2/465	0.000	-0.46±0.01	-0.81±0.01	69.4±1.2
r2-67	08-Jan-2002	ACIS-I	2897	180	pl	1.1±0.8	2.7±0.4	...	11.87/14	0.617	0.19±0.08	-0.40±0.12	34.6±2.6
r2-72	19-Nov-2001	ACIS-I	1585	11	-0.09±0.31	-1.01±0.59	4.9±1.5
r3-8	25-Jun-2000	XMM	0112570401	1426/477/461	nsa	2.7 ^{+0.2} _{-0.2}	...	5.294 ^{+0.010} _{-0.005}	161.37/149	0.231	-1±0.04	-1.01±0.05	310.0±60.0
r3-8	29-Jul-2000	ACIS-I	311	17	-1.04±0.35	-1.08±0.37	160.6±43.3
r3-8	27-Dec-2000	XMM	0112570601	55/ ... /	-0.92±0.27	-0.92±0.27	2.7±0.5
r3-8	29-Jun-2001	XMM	0109270101	110/ ... / ...	nsa	1.1 ^{+0.7} _{-0.3}	...	5.150 ^{+0.070} _{-0.080}	14.24/16	0.582	-0.9±0.26	-0.72±0.27	4.6 ^{+57.2} _{-4.6}
r3-8	31-Aug-2001	ACIS-I	1577	12	-1.01±0.41	-1.01±0.41	27.2±7.9
r3-8	05-Oct-2001	ACIS-S	1575	99	nsa	1.1±0.0	...	5.360±0.020	12.36/9	0.194	-0.80±0.13	-0.91±0.14	36.5±4.9

Table 2—Continued

Source	Date	Inst	OBSID	Counts ^a	Model ^b	N _H ^c	Γ^d	kTorlog(T) ^e	χ^2/ν	Q ^f	HR-1 ^g	HR-2 ^h	L _X ⁱ
r3-8	07-Dec-2001	ACIS-I	2895	5	-1.01±0.65	-1.02±0.65	44.4±20.4
r3-8	06-Jan-2002	XMM	0112570101	1938/415/396	nsa	3 ^{+0.2} _{-0.2}	...	5.310 ^{+0.020} _{-0.010}	133.72/101	0.016	-1±0.03	-0.98±0.03	260.0±68.0
r3-8	08-Jan-2002	ACIS-I	2897	6	-1.00±0.58	-1.00±0.58	52.6±21.9
r3-8	02-Jun-2002	ACIS-I	2898	19	-1.00±0.33	-1.00±0.33	164.6±38.0
r3-16	13-Oct-1999	ACIS-I	303	451	pl	2.6±0.7	2.0±0.2	...	15.16/19	0.713	0.49±0.06	0.18±0.08	38.1±1.9
r3-16	27-Dec-1999	ACIS-I	306	16	-0.35±0.87	0.41±0.45	4.6±1.3
r3-16	29-Jan-2000	ACIS-I	307	14	0.92±1.16	0.97±0.58	4.2±1.3
r3-16	13-Dec-2000	ACIS-I	1581	22	0.42±0.40	-0.73±0.91	2.6±0.8
r3-16	18-Feb-2001	ACIS-I	1582	25	0.34±0.27	0.36±0.27	7.3±1.4
r3-16	29-Jun-2001	XMM	0109270101	90/ ... / ...	pl	0.3 ^{+1.1} _{-0.3}	2.5 ^{+1.0} _{-0.6}	...	32.767/31	0.381	-0.46±0.3	-0.85±0.44	0.8 ^{+0.4} _{-0.3}
r3-16	31-Aug-2001	ACIS-I	1577	5	0.52±0.59	0.00±1.00	0.9±0.4
r3-16	19-Nov-2001	ACIS-I	1585	255	pl	3.3±1.2	1.9±0.2	...	16.48/21	0.742	0.63±0.09	0.45±0.10	55.3±3.5
r3-16	07-Dec-2001	ACIS-I	2895	258	pl	1.3±0.8	1.4±0.2	...	19.37/21	0.562	0.45±0.09	0.45±0.09	44.0±2.7
r3-16	06-Jan-2002	XMM	0112570101	4069/1016/1366	pl	1.5 ^{+0.1} _{-0.1}	1.8 ^{+0.0} _{-0.0}	...	324.2/299	0.151	0.06±0.03	-0.13±0.03	38.6±1.1
r3-16	08-Jan-2002	ACIS-I	2897	230	pl	1.7±0.8	1.8±0.2	...	26.74/19	0.111	0.48±0.09	0.35±0.10	38.3±2.5
r3-16	06-Feb-2002	ACIS-I	2896	29	0.91±0.33	0.80±0.47	5.4±1.1
r3-16	02-Jun-2002	ACIS-I	2898	9	0.43±0.41	-0.00±0.50	1.9±0.6
r3-43	29-Jul-2000	ACIS-I	311	81	dbb	8.6±3.5	...	0.591±0.130	7.87/6	0.248	0.90±0.18	0.69±0.31	25.5±2.9
r3-115	05-Oct-2001	ACIS-S	1575	64	-1±1	-1±1	0.9±0.2
r3-115	07-Dec-2001	ACIS-I	2895	19	0.17±0.29	0.09±0.30	3.2±0.8
r3-115	06-Jan-2002	XMM	0112570101	162/597/742	pl	0.18 ^{+0.15} _{-0.12}	1.8 ^{+0.1} _{-0.1}	...	93.72/66	0.014	15.2 ^{+1.2} _{-1.1}
r3-115	08-Jan-2002	ACIS-I	2897	15	0.34±0.31	0.00±0.36	10.9±2.8
r3-115	06-Feb-2002	ACIS-I	2896	96	pl	0.5±1.5	1.4±0.4	...	4.69/6	0.584	0.42±0.13	0.23±0.15	16.0±1.6
r3-115	02-Jun-2002	ACIS-I	2898	19	0.09±0.30	0.23±0.29	3.6±0.8
r3-125	27-Dec-2000	XMM	0112570601	154/79/75	pl	3.5 ^{+2.7} ₋₂	2.1 ^{+0.7} _{-0.6}	...	22.79/27	0.696	0.29±0.13	0.02±0.16	17.8±5.6
r3-125	13-Jan-2001	ACIS-S	1854	35	0.83±0.29	0.78±0.32	23.2±4.3

Table 2—Continued

Source	Date	Inst	OBSID	Counts ^a	Model ^b	N _H ^c	Γ^d	kTorlog(T) ^e	χ^2/ν	Q ^f	HR-1 ^g	HR-2 ^h	L _X ⁱ
r3-125	29-Jun-2001	XMM	0109270101	458/326/312	pl	$5.6^{+0.7}_{-0.7}$	$2.2^{+0.1}_{-0.1}$...	82.64/80	0.398	0.61±0.11	0.48±0.14	22.7±2.0
r3-126	25-Jun-2000	XMM	0112570401	... /937/851	bb	$1.1^{+0.1}_{-0.1}$...	$0.064^{+0.003}_{-0.003}$	81.93/56	0.014	-0.95±0.05	-0.97±0.06	115.0±18.0
r3-128	29-Jun-2001	XMM	0109270101	318/42/51	bb	$1.7^{+0.1}_{-0.1}$...	$0.024^{+0.004}_{-0.004}$	91/79	0.167	-0.93±0.1	-1.01±0.12	94.0±5.0
s1-1	08-Mar-2001	ACIS-S	2050	325	pl	1.3±0.5	1.9±0.2	...	31.43/26	0.213	0.27±0.07	-0.03±0.08	19.3±1.1
s1-1	03-July-2001	ACIS-I	1584	99	pl	1.0±1.1	1.7±0.3	...	2.79/7	0.903	0.31±0.13	0.20±0.14	16.3±1.6
s1-1	05-Oct-2001	ACIS-I	1576	99	pl	0.6±1.3	1.2±0.4	...	7.43/5	0.190	0.54±0.15	0.46±0.16	16.3±1.6
s1-1	12-Jan-2002	XMM	0112570201	1334/426/458	pl	$1.4^{+0.2}_{-0.2}$	$1.7^{+0.1}_{-0.1}$...	170.63/148	0.098	0.06±0.05	-0.14±0.06	22.0±1.1
s1-18	21-Sep-2000	ACIS-S	313	22	-0.94±0.25	-1.16±0.32	57.0±16.0
s1-18	05-Nov-2000	ACIS-S	2049	70	nsa	1.6±0.5	...	5.170±0.056	2.43/4	0.657	-0.97±0.18	-1.00±0.19	22.6±2.8
s1-27	3-Jul-2001	ACIS-S	2051	22	-0.20±0.32	-1.02±0.59	0.6±0.2
s1-69	3-Jul-2001	ACIS-S	2051	14	-1.12±0.49	-0.56±0.34	1.0±0.3
s1-80	08-Jul-2002	ACIS-I	2901	527	dbb	1.3±0.5	...	0.741±0.064	12.34/20	0.904	0.52±0.06	0.01±0.07	75.1±3.3
s1-80	23-Aug-2002	ACIS-I	2899	179	dbb	1.1±0.8	...	0.452±0.072	10.05/13	0.690	0.34±0.08	-0.58±0.14	21.5±1.6

Table 2—Continued

Source	Date	Inst	OBSID	Counts ^a	Model ^b	N _H ^c	Γ ^d	kTorlog(T) ^e	χ ² /ν	Q ^f	HR-1 ^g	HR-2 ^h	L _X ⁱ
--------	------	------	-------	---------------------	--------------------	-----------------------------	----------------	-------------------------	-------------------	----------------	-------------------	-------------------	-----------------------------

^aThe number of net counts in the detection. XMM detection counts are given for 0.3–7 keV in PN/MOS1/MOS2 format.

^bThe model used to fit the spectrum: pl (power-law), bb (blackbody), (pb) power-law plus blackbody, (dbb) disk blackbody, (nsa) neutron star atmosphere.

^cThe absorption value in units of 10²¹ cm^{−2}

^dSlope of the best-fitting power law component.

^eFor the bb or pb models, this number is kT in keV. For the dbb model this value is kT in keV of the inner edge of the accretion disk. For the nsa model this value is $\log(T_{eff})$ for the atmosphere of the neutron star.

^fThe probability that this fit is representative of the true spectrum, determined from χ^2/dof .

^gHardness ratio calculated by taking the ratio of M-S/M+S, where S is the number of counts from 0.3–1 keV and M is the number of counts from 1–2 keV.

^hHardness ratio calculated by taking the ratio of H-S/H+S, where S is the number of counts from 0.3–1 keV and H is the number of counts from 2–7 keV.

ⁱThe absorption-corrected luminosity of the source in units of 10³⁶ erg s^{−1} (0.3–7 keV), assuming a distance of 780 kpc.

Table 3. Lightcurve Properties

Source	Peak Date ^a	L_X ^b	UL ^c	Hi/Lo ^d	Decay Start ^e	N_{LC} ^f	τ_d ^g	χ_ν^{2h}	N ⁱ	DC ^j	Type
n1-26	2001-07-03	1.1±0.4	0.66	2	2001-07-03	QSS
n1-59	2000-10-12	18.8±7.9	0.84	22	2000-10-12	3	5	1.0	2	0.03	LDC
n1-85	2001-10-31	62.8±12.6	0.16	397	2001-10-31	5	8	1.8	1	<0.02	LDC
n1-86	2002-02-06	2018.4±246.6	25.54	79	2002-02-06	1	...	LDC
n1-87	2001-10-31	29.3±27.6	10.48	3	2001-10-31	4	50	1.5	1	...	LDC
n1-88	2001-11-19	14.7±6.6	0.32	45	2001-11-19	4	14	3.0	1	<0.04	LDC
n1-89	2000-05-26	9.6±4.7	3.30	3	2000-05-26	5	110	0.3	LDC
r1-5	2000-01-19	200.5±24.0	0.70	285	2000-01-19	21	200	21.7	1	<0.47	LD
r1-9	2000-02-16	89.2±12.5	5.60	16	2000-02-16	3	30	2.2	HDC
r1-11	1999-12-11	23.6±3.6	3.54	7	1999-12-27	7	86	0.7	4	...	HDC
r1-19	2000-10-12	17.0±7.3	2.43	7	2000-10-12	3	30	0.1	1	...	MDC
r1-23	2000-08-27	21.9±4.0	2.02	11	2000-08-27	6	100	5.9	HDC
r1-28	2000-03-08	11.6±4.1	0.53	22	2000-03-08	3	40	0.6	1	<0.07	LDC
r1-34	2001-10-31	85.8±2.6	2.31	37	2001-10-31	5	19	11.2	1	<0.04	LDC
r1-35	2001-10-05	3.1±0.3	1.03	3	2001-10-05	SSS
r2-3	2000-10-12	65.4±10.9	1.99	33	2000-12-13	HDC
r2-8	1999-10-13	25.5±1.3	0.10	260	1999-10-13	3	20	0.1	2	0.10	MDC
r2-16	2001-06-10	40.8±15.4	0.26	158	2001-06-10	7	41	0.8	4	0.34	MDC
r2-28	2000-01-29	13.4±1.6	0.07	186	2000-01-29	5	15	0.7	1	<0.03	LDC
r2-29	2000-06-21	30.7±7.7	0.12	262	2000-06-21	8	20	2.3	1	<0.05	LDC
r2-60	2001-10-05	451.6±41.0	8.80	51	2001-10-05	2	<92	...	1	...	MDC/SSS
r2-61	2001-10-05	1.0±0.1	0.03	33	2001-10-05	2	<92	...	1	...	SSS
r2-63	2002-01-06	29.0±1.4	0.40	72	2002-01-06	MDC/SSS
r2-65	2001-01-13	1.9±0.6	0.11	17	2001-01-13	4	60	7.0	2	0.32	SSS
r2-67	2001-10-05	315.5±2.2	0.15	2163	2001-10-05	10	50	115.8	1	<0.12	LDC
r2-69	2000-10-12	29.8±9.0	0.12	248	2000-10-12	3	20	0.3	2	0.10	MDC

Table 3—Continued

Source	Peak Date ^a	L_X ^b	UL ^c	Hi/Lo ^d	Decay Start ^e	N_{LC} ^f	τ_d ^g	χ_ν^{2h}	N ⁱ	DC ^j	Type
r2-72	2001-11-19	4.9±1.5	0.23	22	2001-11-19	3	10	0.1	1	<0.03	LDC
r3-8	2000-06-25	310.0±60.0	3.23	96	2000-06-25	5	3	5.3	4	0.02	MDC
r3-16	2001-11-19	68.4±17.5	0.64	107	2001-11-19	7	50	35.1	2	0.21	MDC
r3-43	2000-07-29	25.5±2.9	0.23	112	2000-07-29	3	10	0.9	1	<0.03	LDC
r3-46	2000-08-18	37.4±10.2	0.18	203	2000-08-18	4	22	0.4	2	0.10	LDC
r3-115	2002-01-16	20.0±6.4	0.13	155	2002-01-16	3	80	0.1	1	<0.18	LDC/SSS
r3-125	2000-09-11	26.8±13.7	0.29	93	2000-09-11	10	100	15.8	1	<0.29	LD
r3-126	2000-06-25	115.0±18.0	0.17	694	2000-06-25	3	20	0.2	1	<0.04	LDC
r3-128	2001-06-29	94.0±5.0	2.50	38	2001-06-29	3	40	0.1	1	<0.10	LDC
s1-1	2001-10-31	31.8±11.8	2.44	13	2001-10-31	7	94	1.9	1	...	LD
s1-18	2000-09-21	57.0±16.0	0.38	151	2000-09-21	5	55	0.4	1	<0.39	SSS
s1-27	2001-07-03	0.6±0.2	0.17	4	2001-07-03	2	<192	QSS
s1-69	2001-07-03	1.0±0.3	0.25	4	2001-07-03	2	<192	SSS
s1-79	1999-11-29	154.5±14.0	0.10	1490	1999-11-29	6	70	5.5	1	<0.15	LDC
s1-80	2002-06-02	131.5±14.2	0.09	1481	2002-06-02	5	40	10.9	2	0.14	LDC
s1-82	1999-11-29	16.8±8.2	0.20	85	1999-11-29	4	60	0.2	1	<0.12	LDC

Table 3—Continued

Source	Peak Date ^a	L_X ^b	UL ^c	Hi/Lo ^d	Decay Start ^e	N_{LC} ^f	τ_d ^g	χ_ν^2 ^h	N ⁱ	DC ^j	Type
--------	------------------------	--------------------	-------------------	----------------------	--------------------------	-----------------------	-----------------------	---------------------------	----------------	-----------------	------

^aThe date of the highest measured source luminosity.

^bThe 0.3–7 keV luminosity of the X-ray source at the date given in column 2 in units of 10^{36} erg s^{−1}.

^cThe lowest 0.3–7 keV luminosity upper-limit in the lightcurve of the X-ray source in units of 10^{36} erg s^{−1}.

^dThe ratio of the highest luminosity of the X-ray source observed to the lowest luminosity upper-limit in the lightcurve. The highest luminosity observed can be different from the value in column 3 if the highest luminosity observed did not have a well-sampled decay curve.

^eThe date chosen as the beginning of the source decay curve. Sometimes later than the peak date if the source did not steadily decay after the peak detection.

^fThe number of data points in the decay curve used to estimate the e -folding decay time of the source.

^gThe estimate of the e -folding decay time of the source in days.

^hThe χ_ν^2 value of the fit to an exponential decay adopting 3σ errors for detections and 1σ errors for upper-limits.

ⁱThe number of distinct outbursts observed.

^jThe duty cycle of the source is estimated for sources with $Hi/Lo > 15$, measured decay times, and at least one clear outburst. Upper-limits for the duty cycle are give for sources that only showed one outburst.

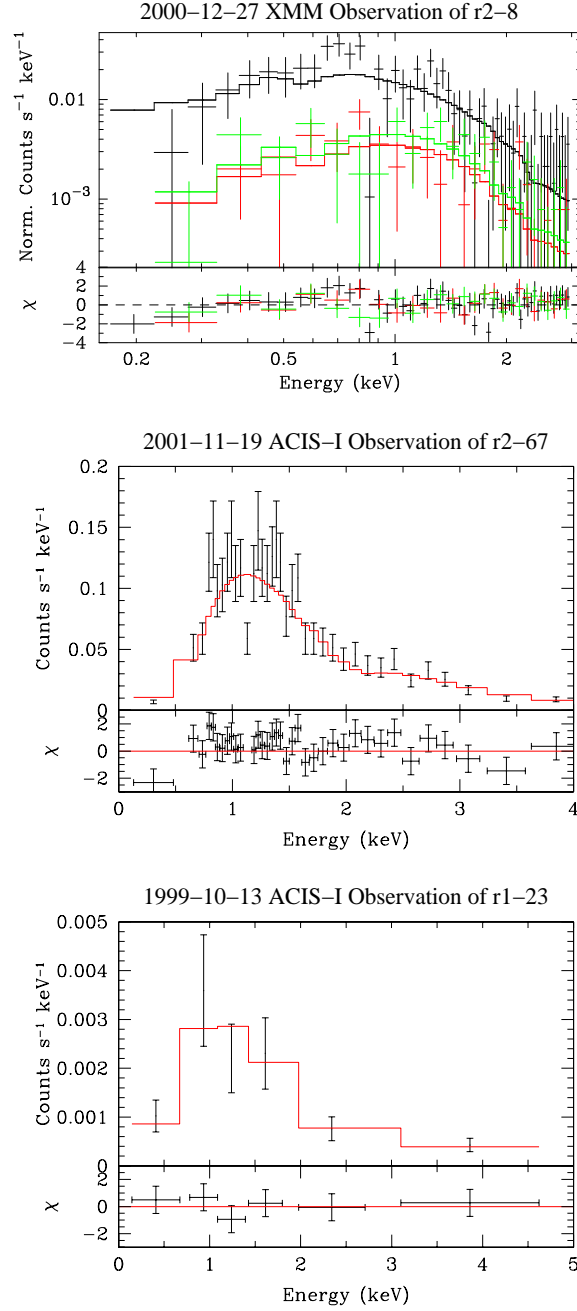


Fig. 1.— A few sample spectral fits are shown. The top plot shows a typical XMM fit. The green and red spectral fits are for the MOS-1 and MOS-2 detectors, and the black fit is for the PN detector. The middle plot shows a typical ACIS fit for a high count rate detection, and the bottom plot shows a typical ACIS fit for a low count rate detection. In all plots, histograms mark the best fit model prediction and error bars mark the measured count rates from the data.

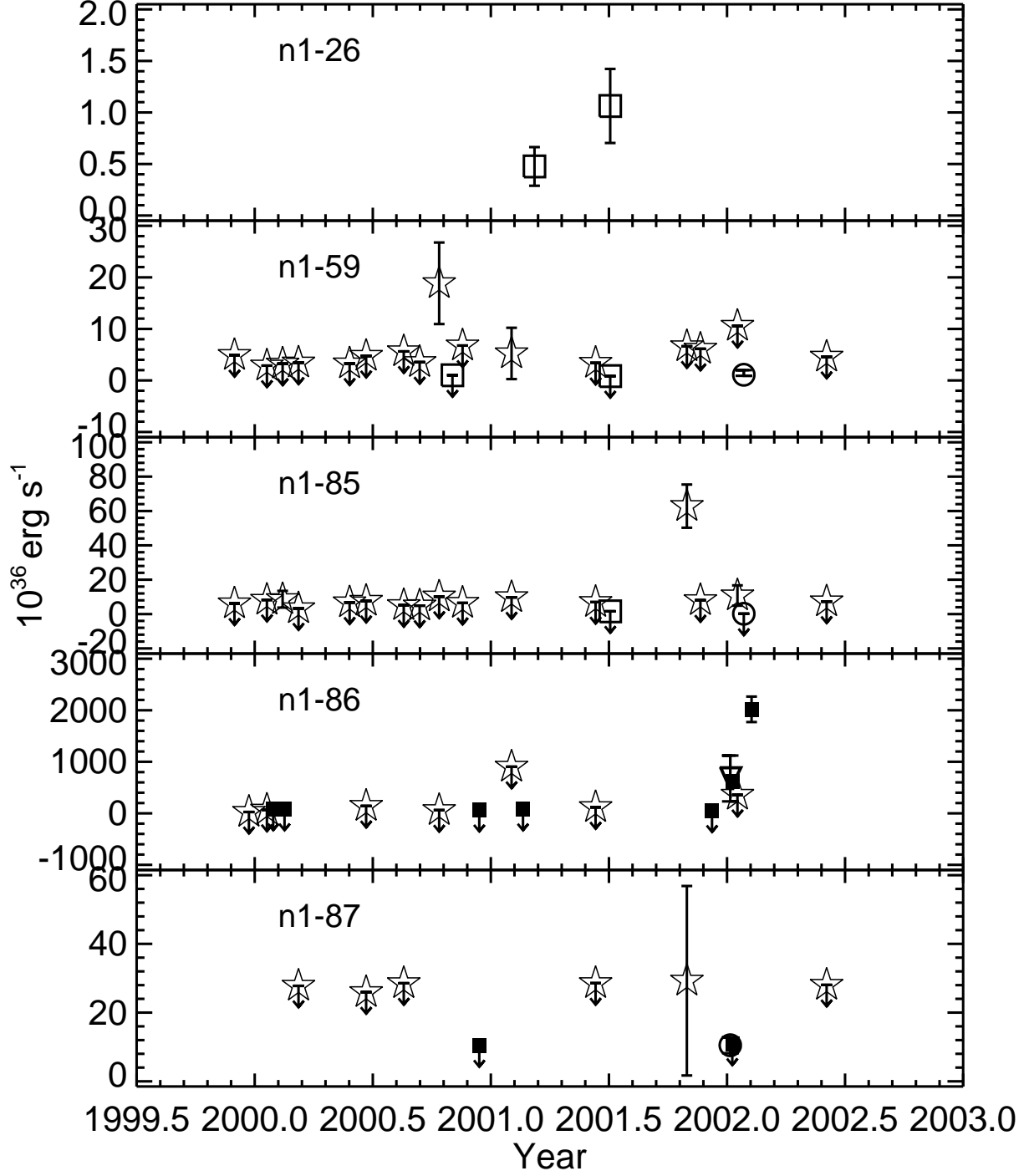


Fig. 2.— The lightcurves of the transient sources. These lightcurves contain data from XMM (circles, triangles mark cases where no PN data was available), ACIS-I (filled squares), ACIS-S (open squares), and HRC (open stars). Upper-limits of non-detections are indicated with arrows.

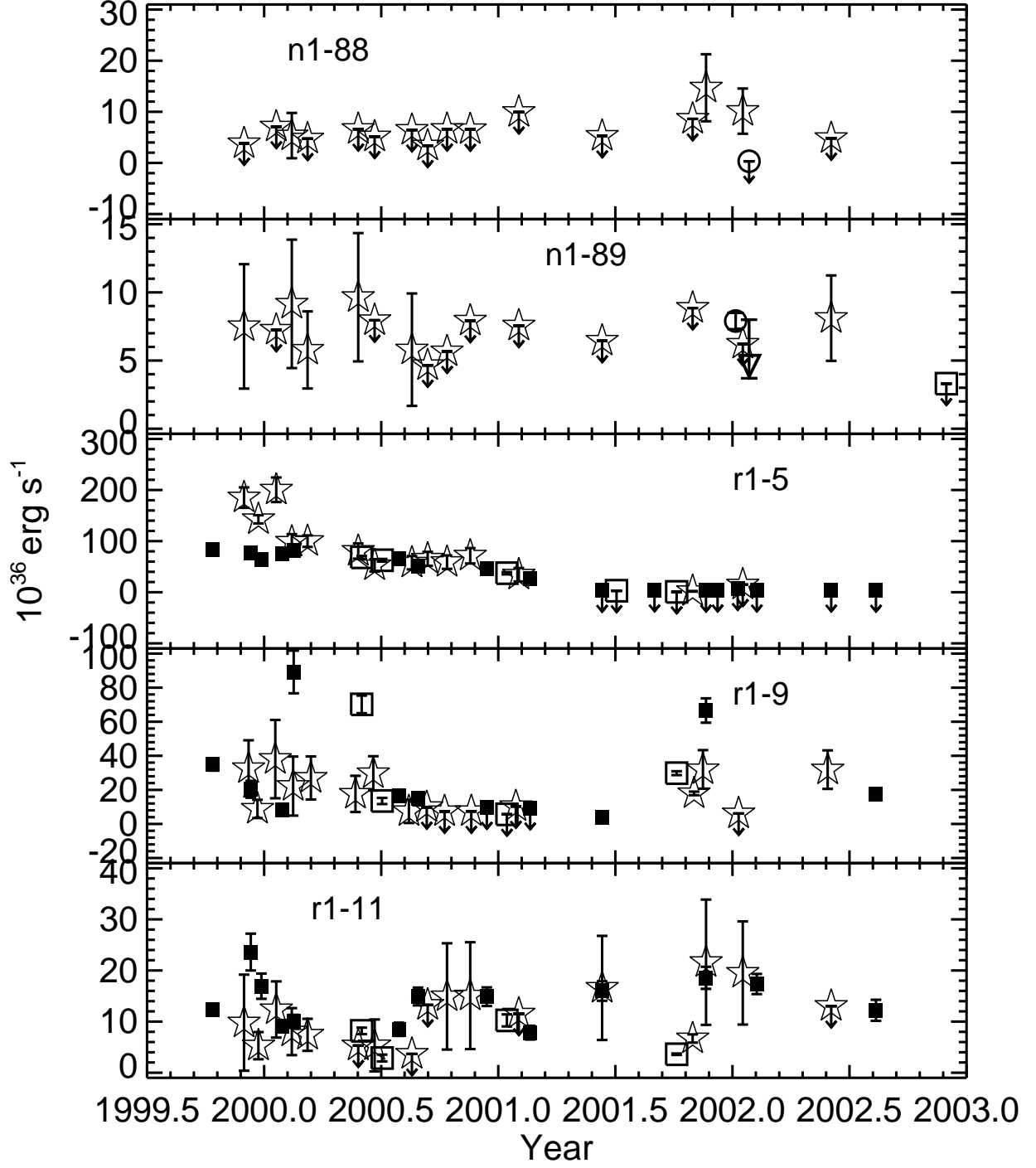


Fig. 3.— The lightcurves of the transient sources. Symbols are the same as Figure 2.

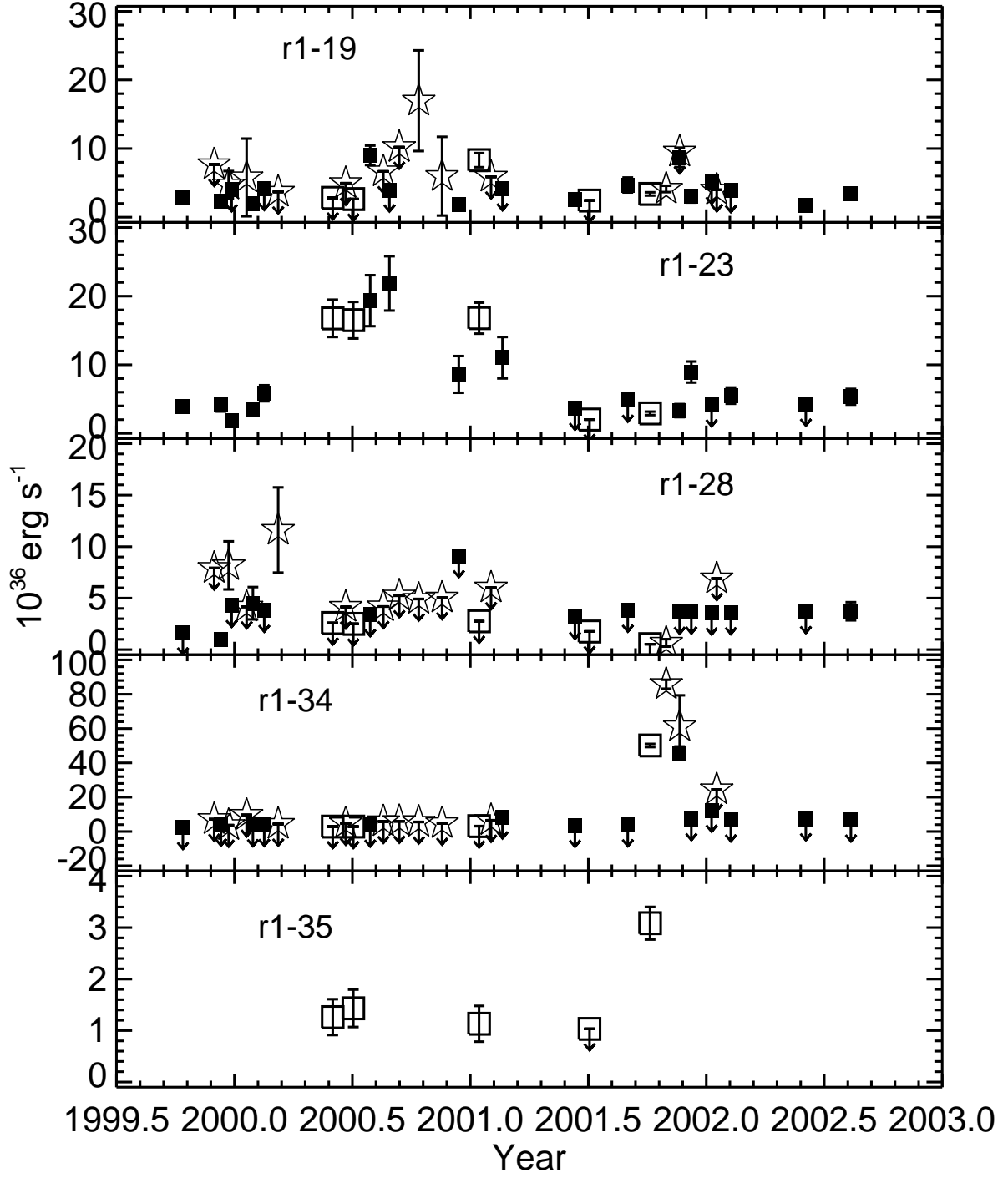


Fig. 4.— The lightcurves of the transient sources. Symbols are the same as Figure 2.

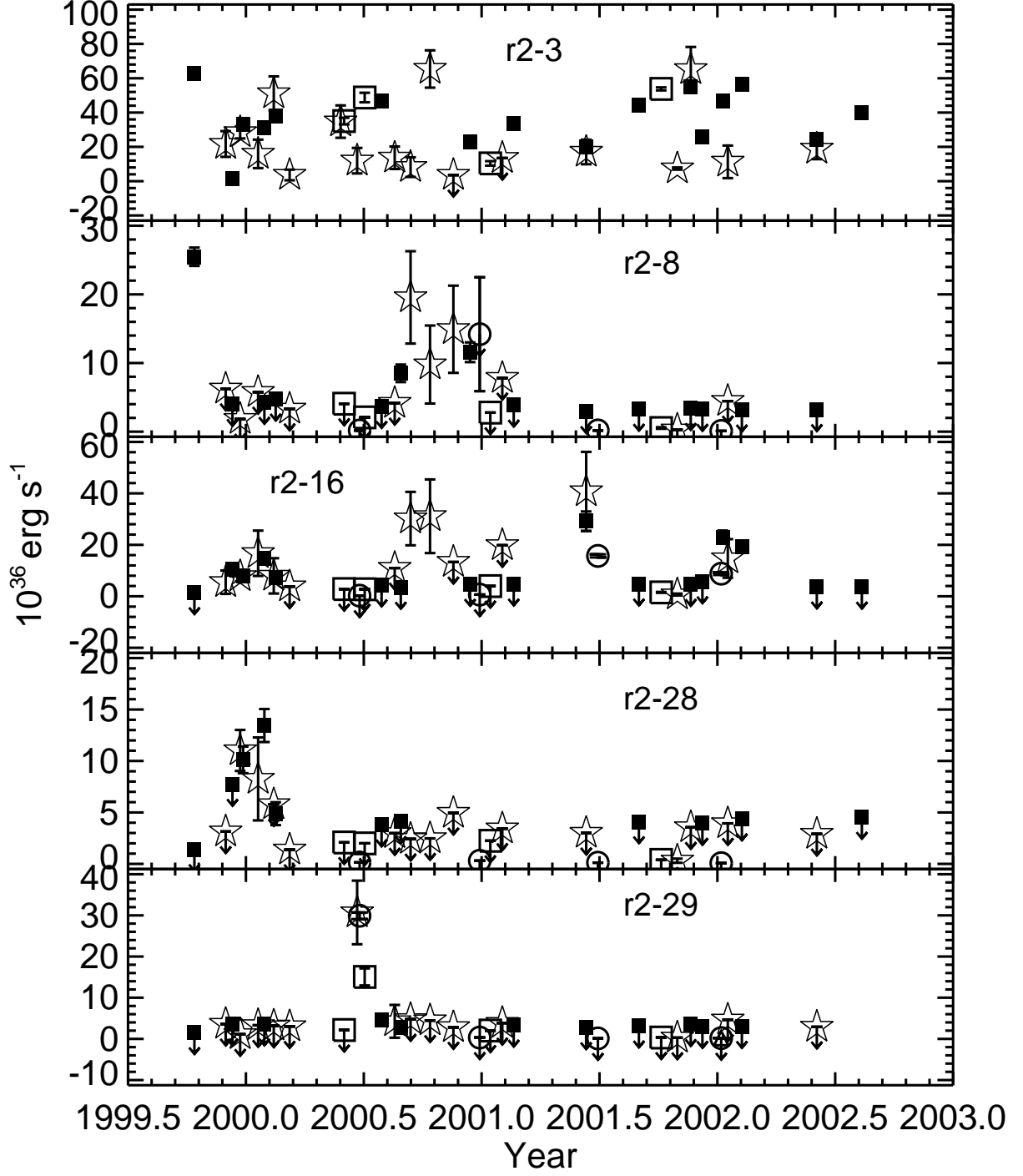


Fig. 5.— The lightcurves of the transient sources. Symbols are the same as Figure 2.

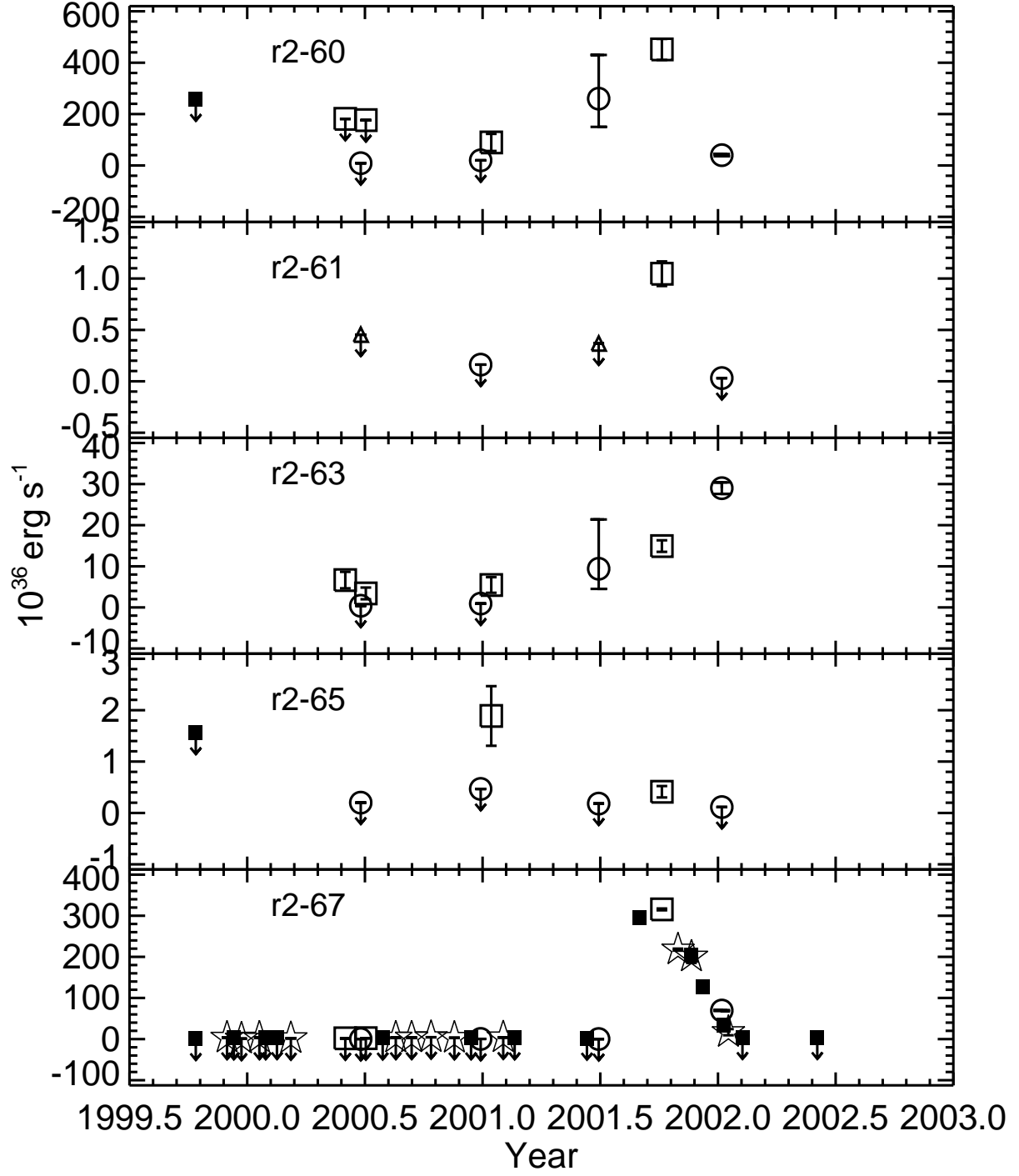


Fig. 6.— The lightcurves of the transient sources. Symbols are the same as Figure 2.

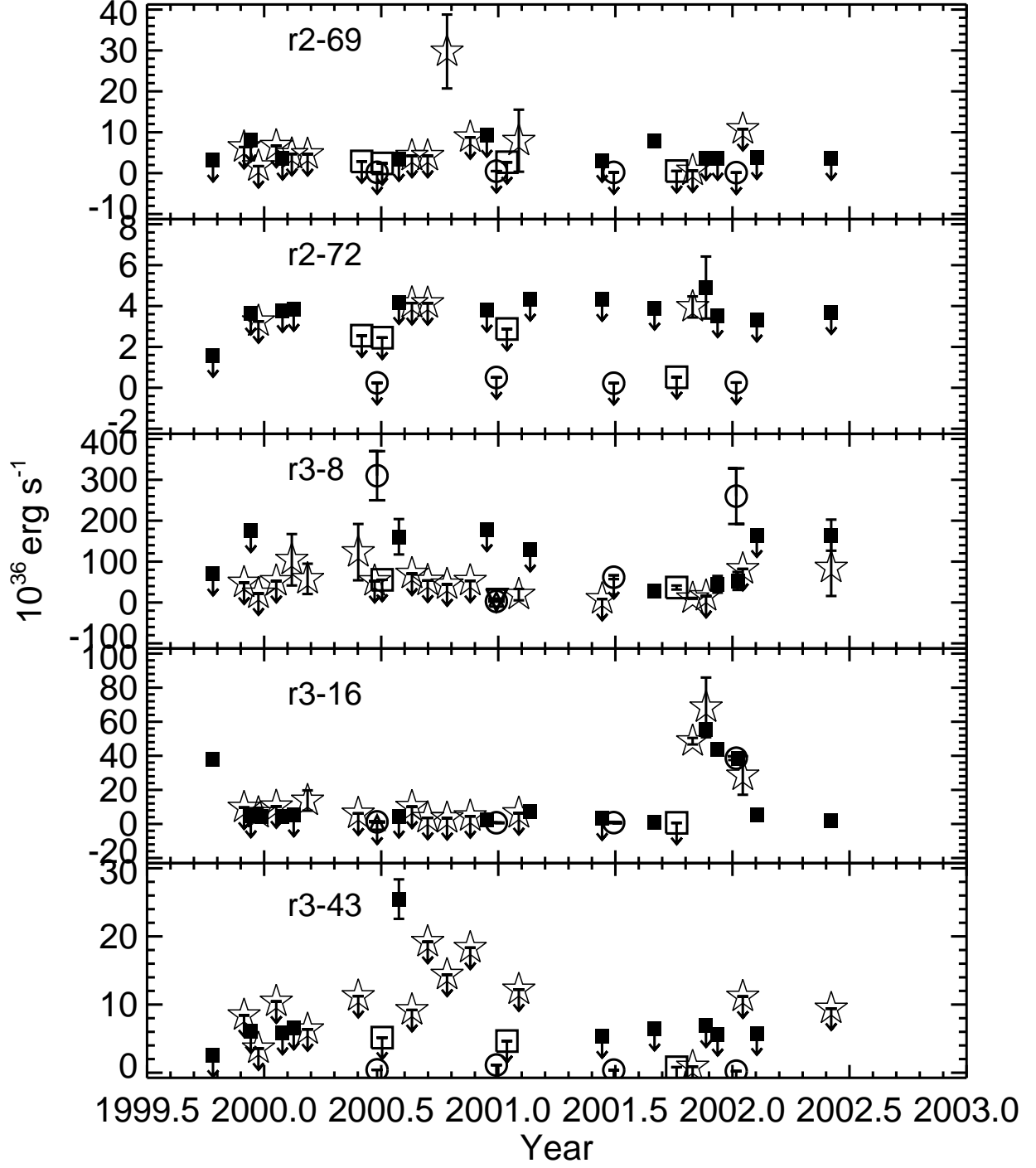


Fig. 7.— The lightcurves of the transient sources. Symbols are the same as Figure 2.

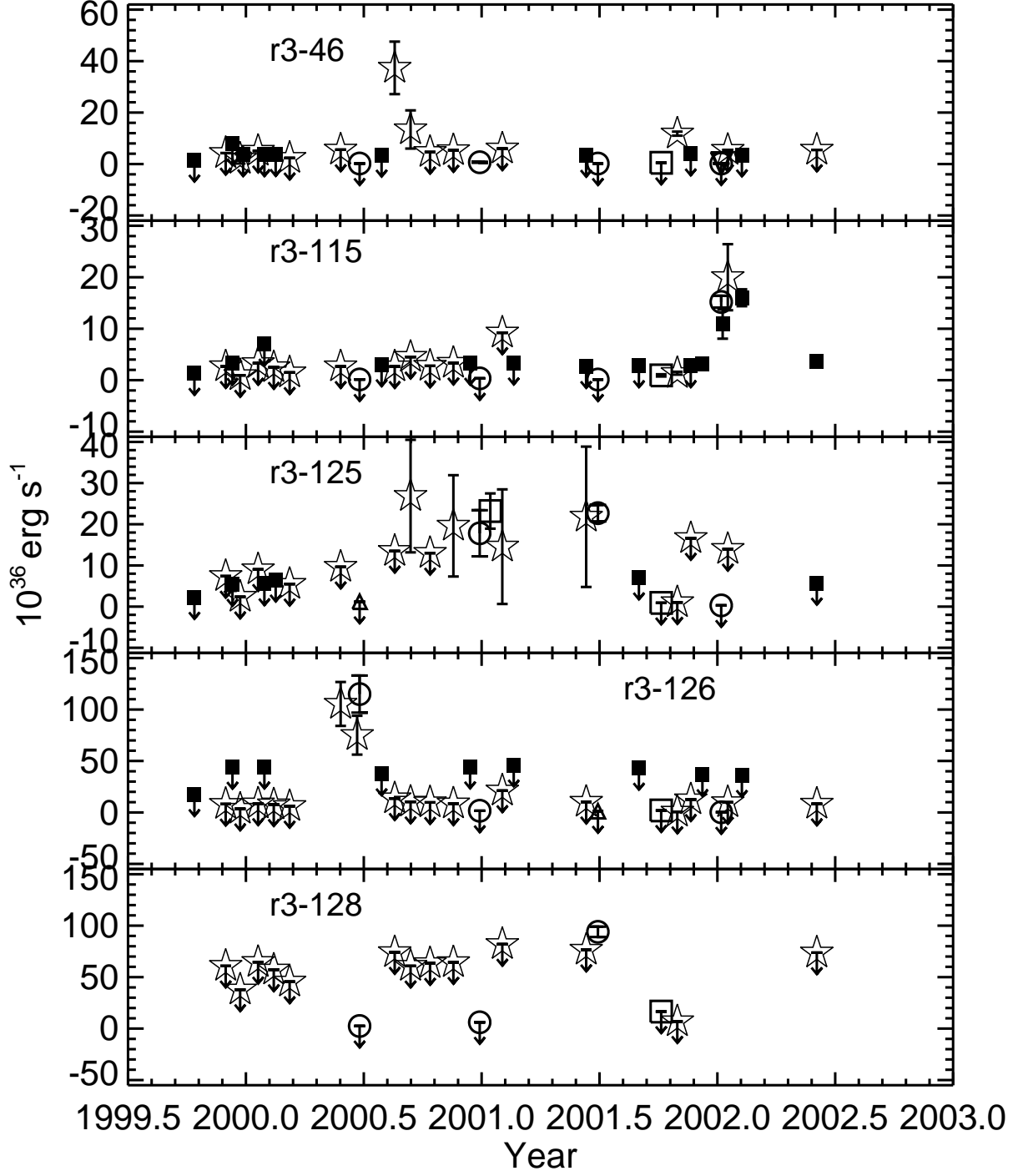


Fig. 8.— The lightcurves of the transient sources. Symbols are the same as Figure 2.

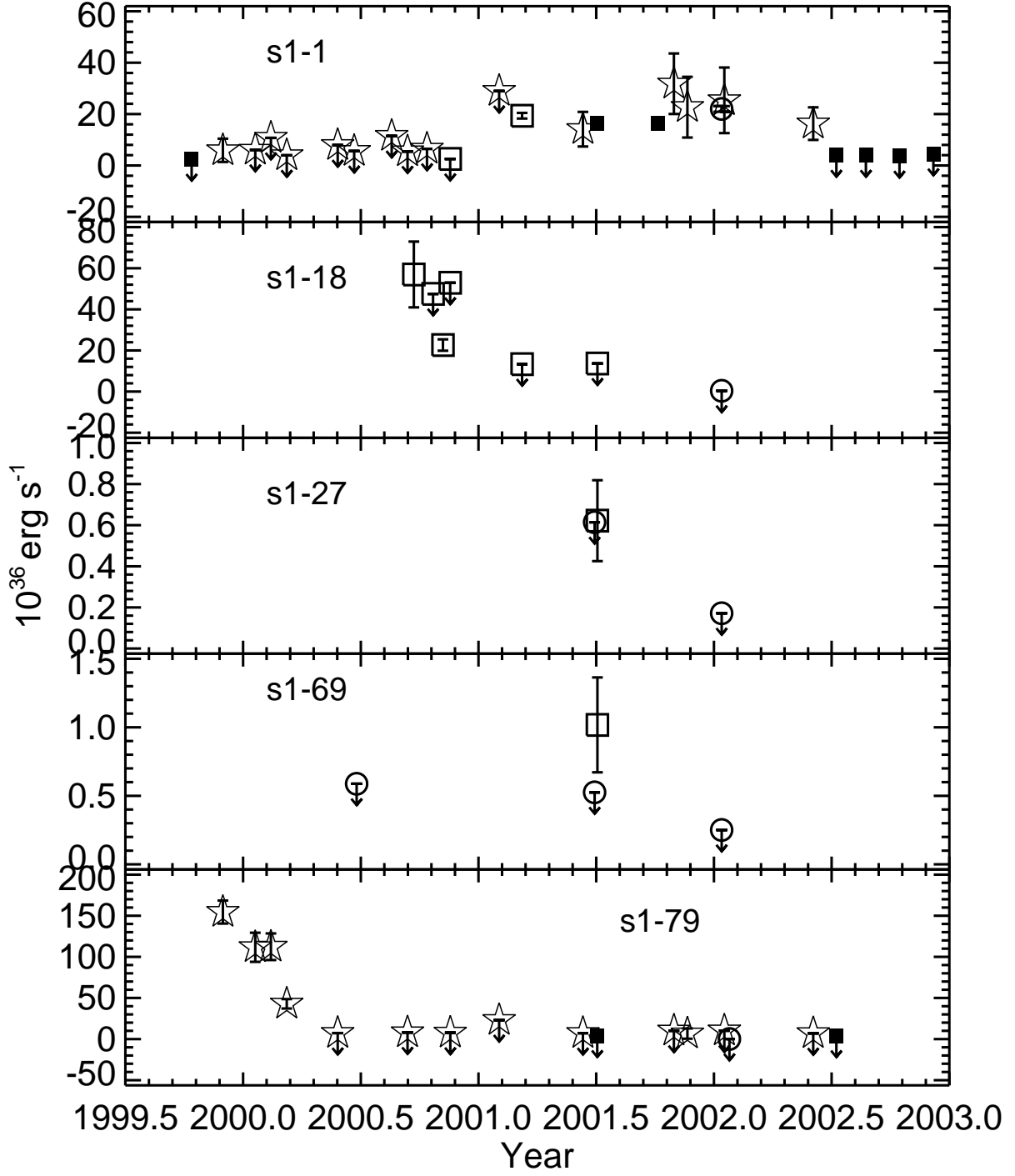


Fig. 9.— The lightcurves of the transient sources. Symbols are the same as Figure 2.

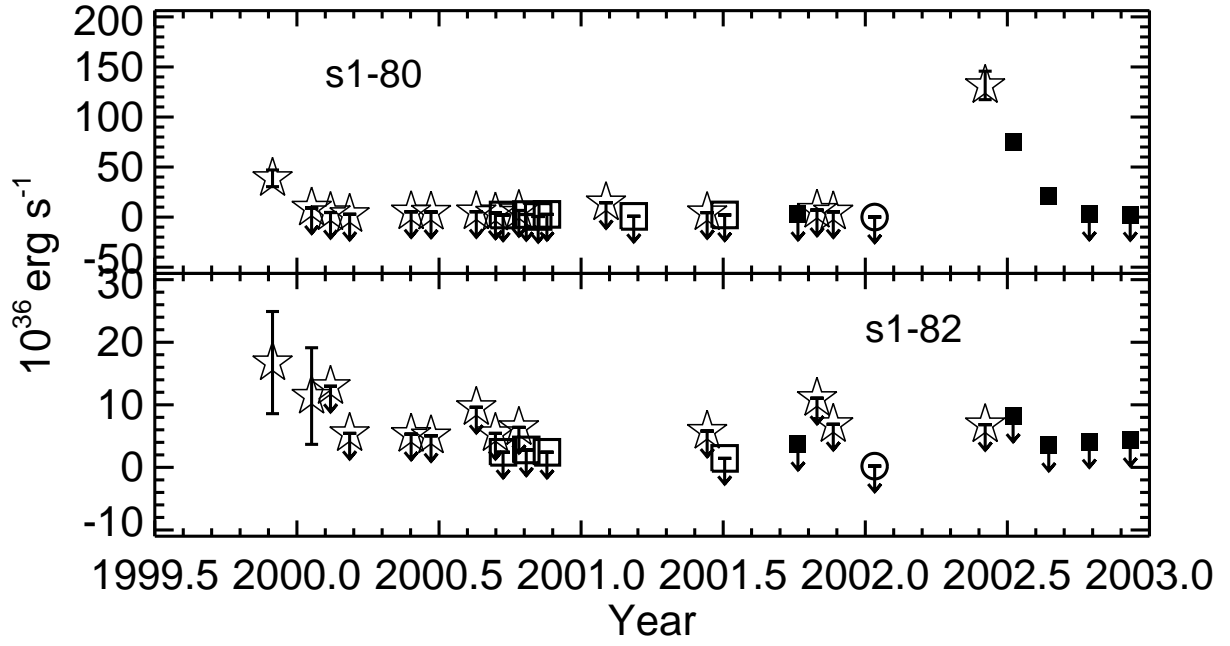


Fig. 10.— The lightcurves of the transient sources. Symbols are the same as Figure 2.

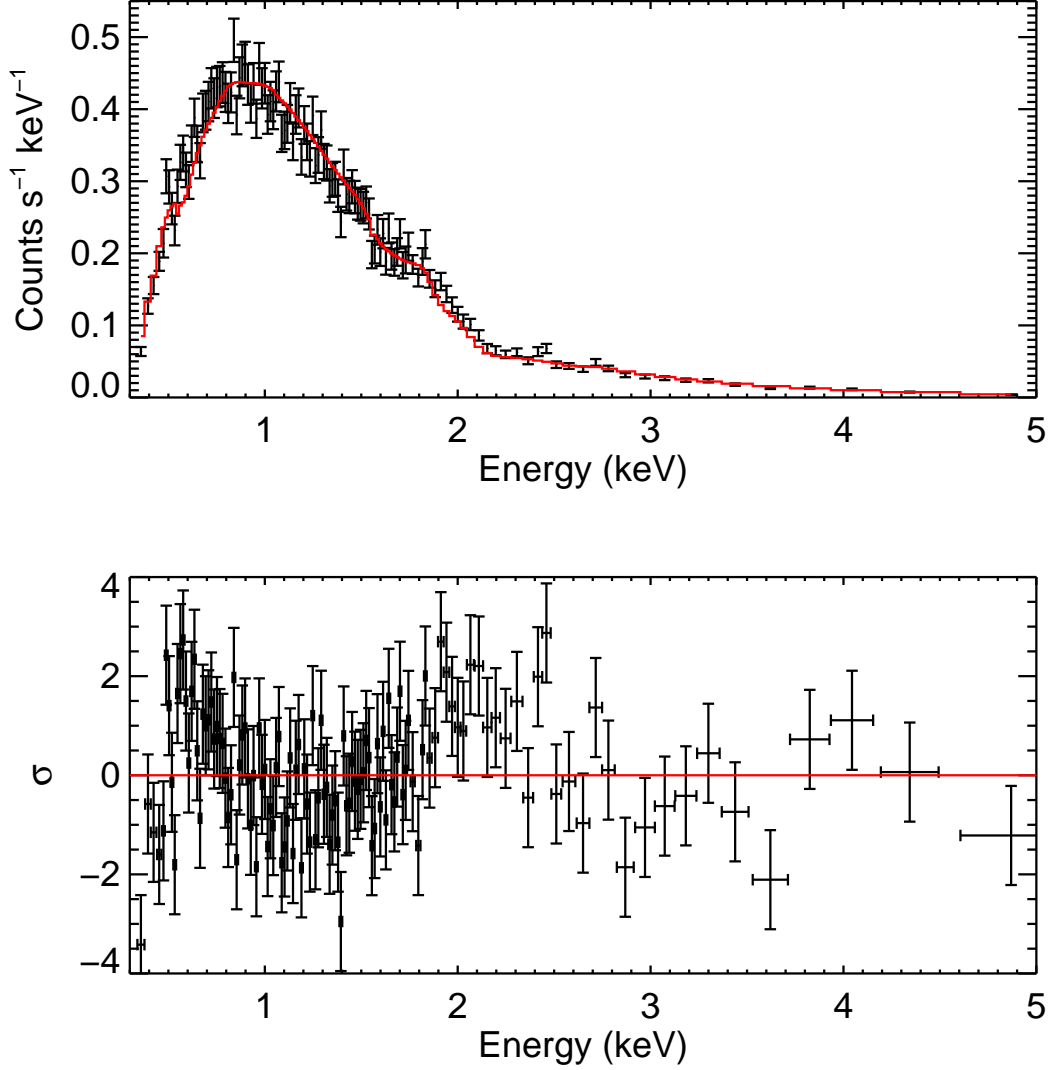


Fig. 11.— The best-fitting model (disk blackbody plus power-law) with pileup for the 05-Oct-2001 (ObsID 1575) observation of r2-67. *Top*: Histogram marks the best fit model prediction and error bars mark the measured count rates from the data. *Bottom*: Error bars mark the residuals between the model and the data in units of σ .

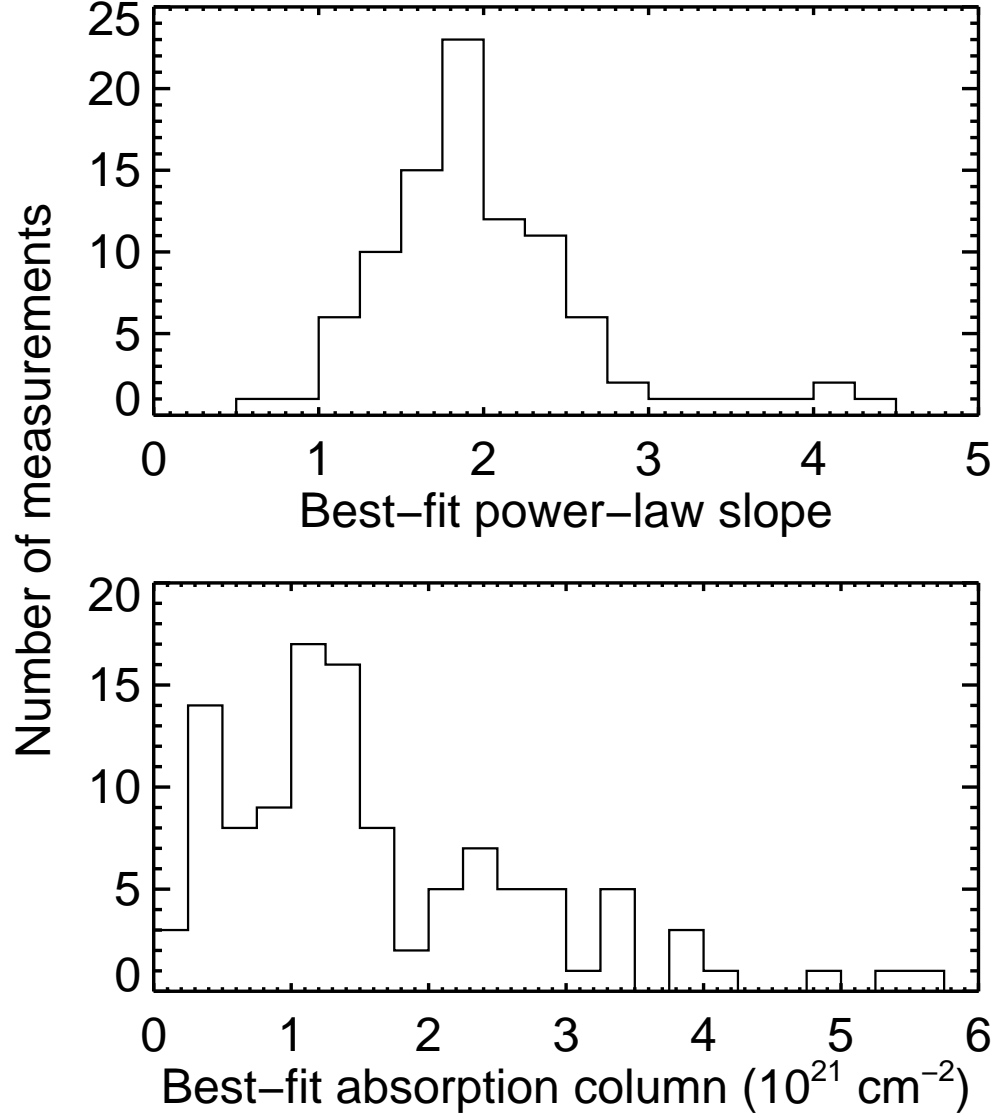


Fig. 12.— *Top*: Histogram of the power-law slope (Γ) measurements for all detections fitted with power-law spectral models. *Bottom*: Histogram of the absorption column measurements for all spectral fits where the absorption was a free parameter and was constrained beyond an upper-limit value.

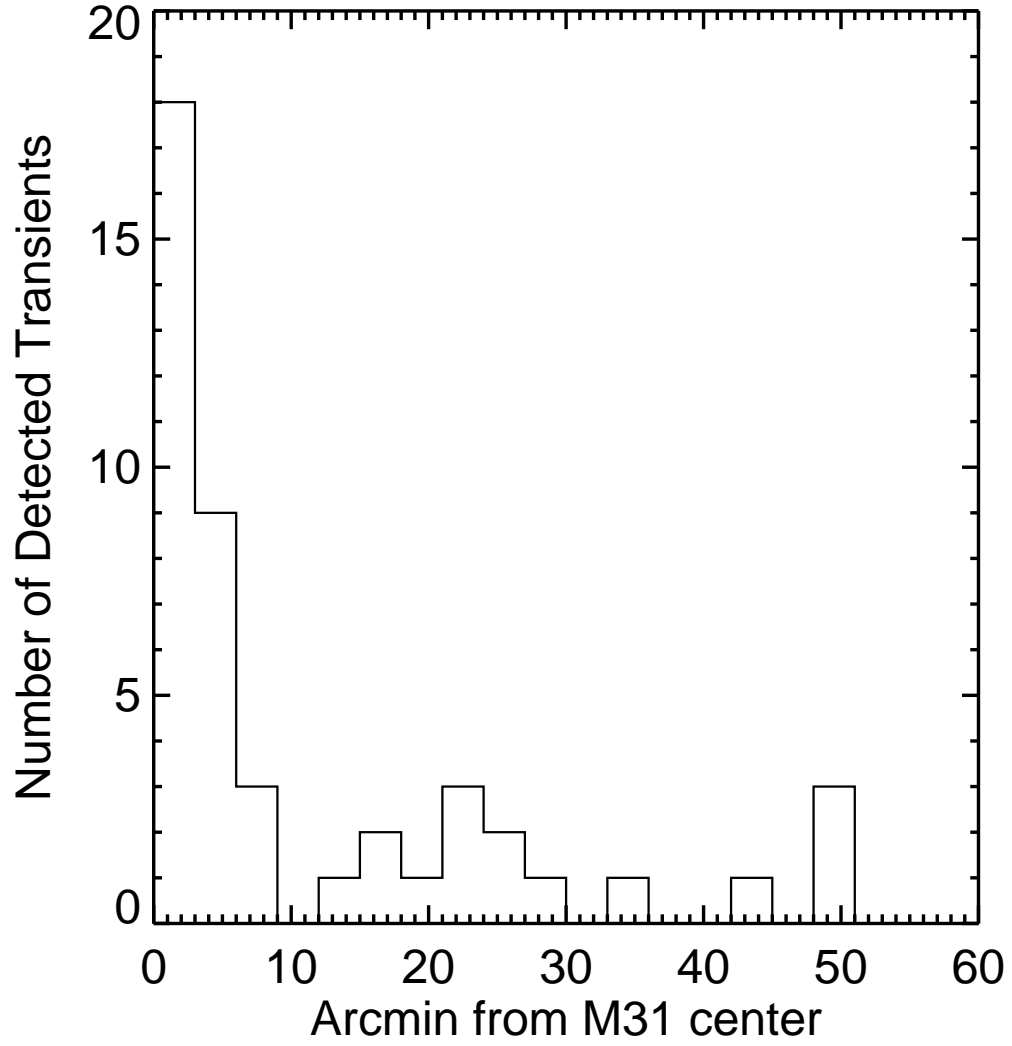


Fig. 13.— A histogram of the number of detected transients as a function of their distance from the center of M31 is shown. The distribution shows a clear peak near the center of the galaxy, suggesting most transient X-ray sources in M31 are old objects.

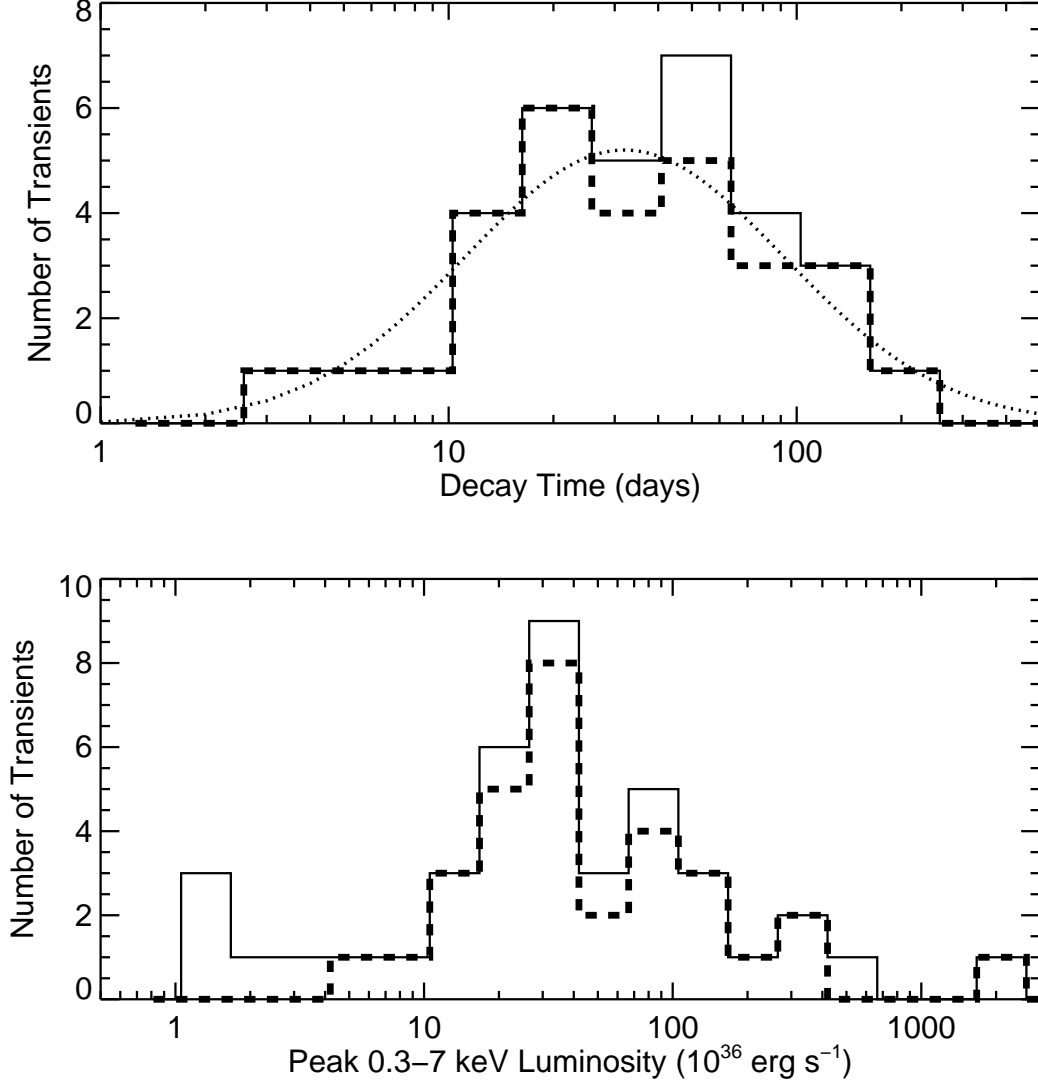


Fig. 14.— *Top*: A histogram of the number of transients as a function of e -folding decay time. *Solid line* gives all transients with measured decay times, and *dashed line* ignores the SSSs and QSSs. *Dotted line* shows best-fitting Gaussian to the distribution. The peak and width of the Gaussian are consistent with the distribution found for Galactic transients by Chen et al. (1997). *Bottom*: A histogram of the number of transients as a function of maximum observed luminosity. *Solid line* gives all transients with at least one single-epoch detection, and *dashed line* ignores the SSSs and QSSs. The single source above $10^{39} \text{ erg s}^{-1}$ is n1-86, a soft source that may be a foreground CV, which would lower its peak luminosity to $< 10^{36} \text{ erg s}^{-1}$.

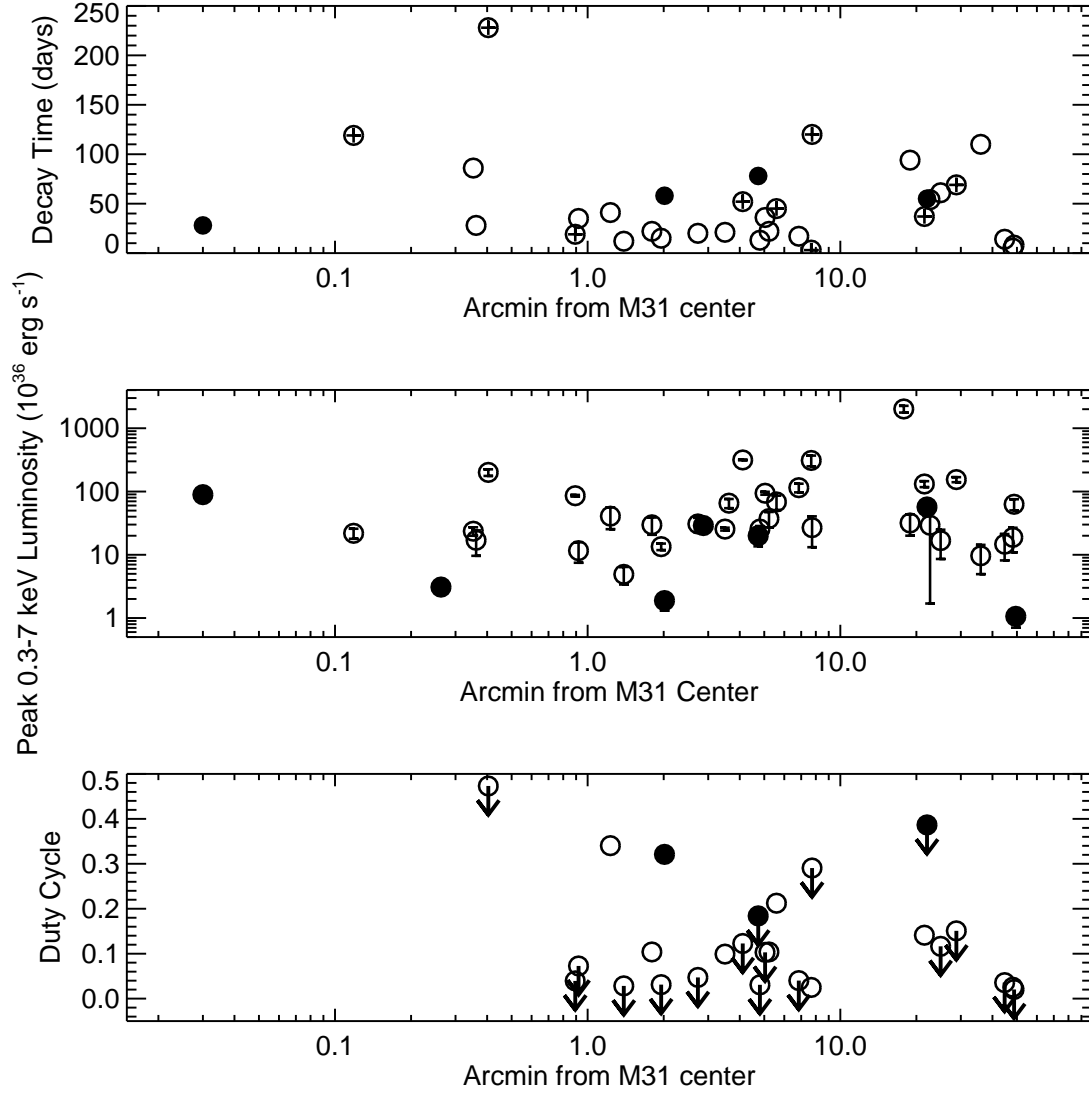


Fig. 15.— *Top:* A plot of the e -folding decay times of the XRTs as a function of their distance from the galaxy center. Filled circles denote SSSs and QSSs. Circles around crosses mark poor fits to an exponential decay ($\chi^2_\nu > 3$). *Middle:* The maximum observed luminosities of the transients as a function of their distance from the galaxy center. Filled circles denote SSSs and QSSs. *Bottom:* The duty cycle estimates of the transients as a function of galactocentric distance. Filled circles denote SSSs and QSSs. Upper-limits are plotted for sources showing only one outburst during the time period studied.

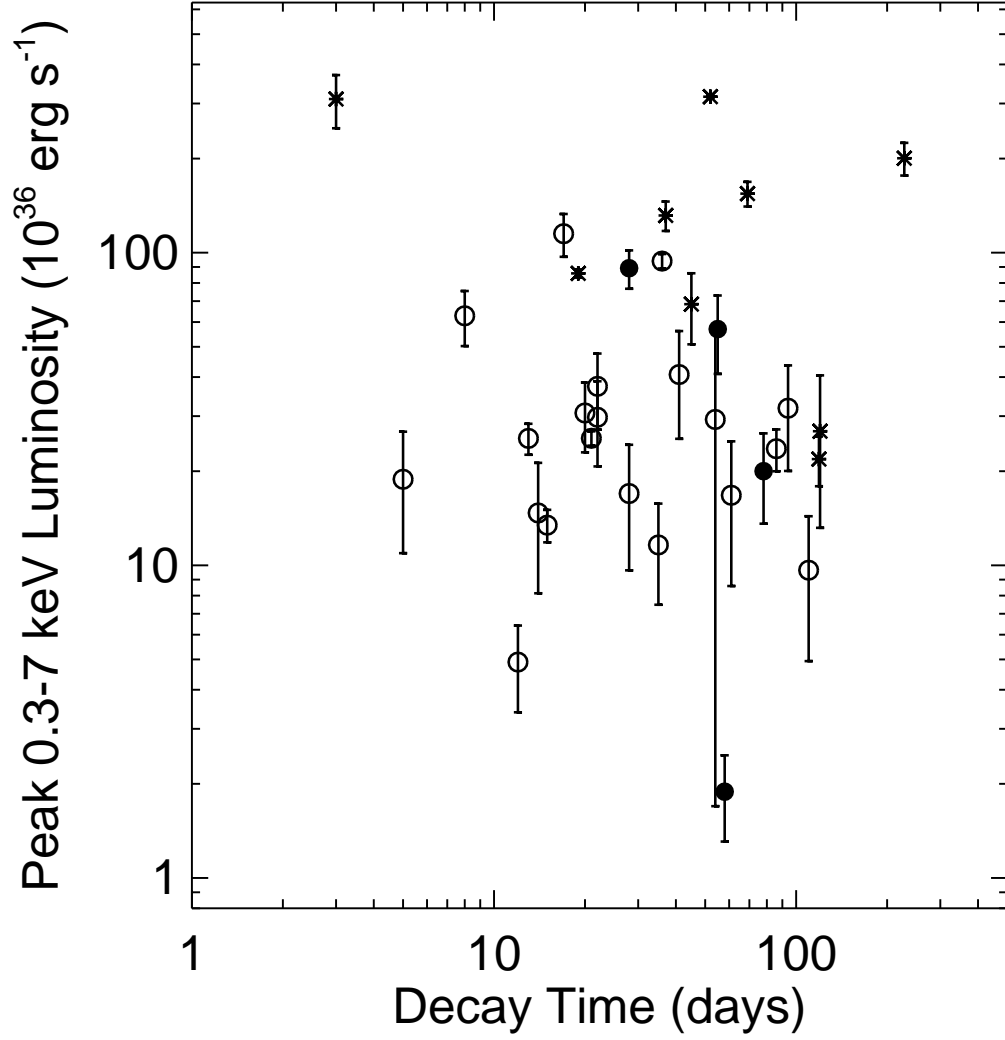


Fig. 16.— The e -folding decay time vs. the peak luminosity. The values cover a similar range in parameter space to those seen in Galactic outbursts (Chen et al. 1997). Filled circles denote SSSs and QSSs. Asterisks mark poor fits to an exponential decay ($\chi^2_\nu > 3$).

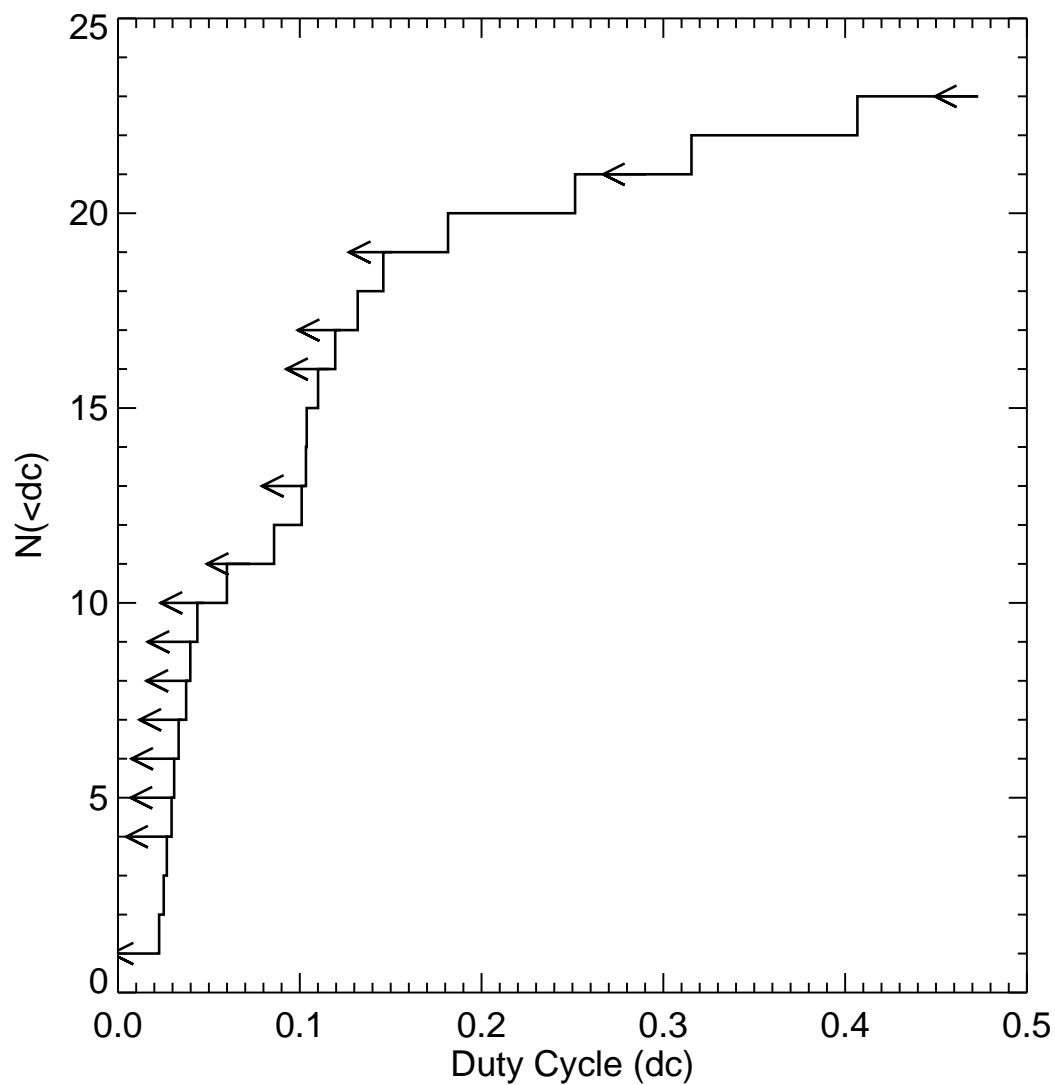


Fig. 17.— The distribution of duty cycles for the 23 non-SSSs with constraints from the available data. The histogram shows the cumulative number of XRTs with duty cycles less than the values given on the abscissa. Upper-limit values are shown with left arrows.

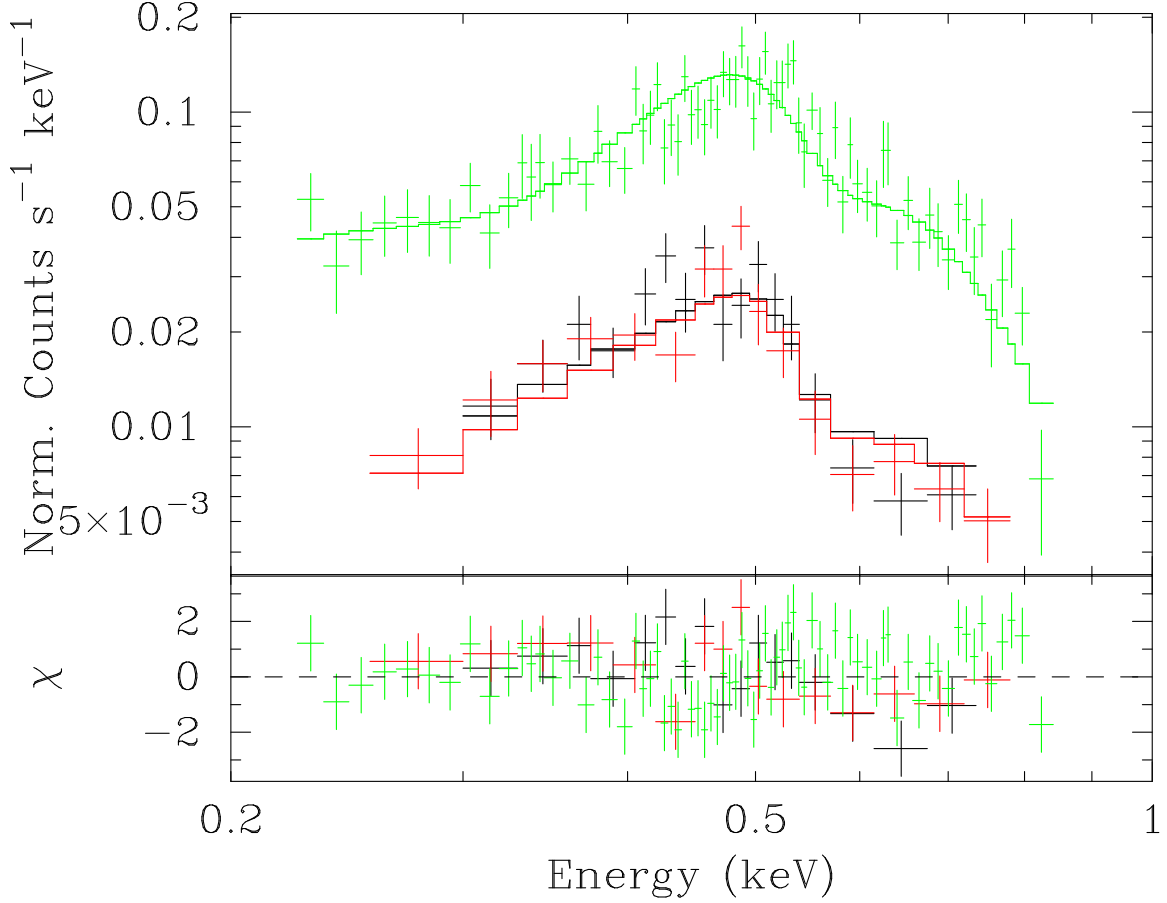


Fig. 18.— The best-fit single-component model for the 2002 January 06 observation of r3-8. *Top*: The green histogram marks the best fit model prediction for the PN detection and error bars mark the measured count rates from the PN data. The red histogram and error bars show the same fit for the MOS 1 data, and the black histogram and error bars show the same fit for the MOS 2 data. *Bottom*: Residuals for the spectral fits. The colors correspond to the same instruments as in *top*. The spectrum was equally well-fit by a multi-component model (absorbed blackbody plus Gaussian emission line).

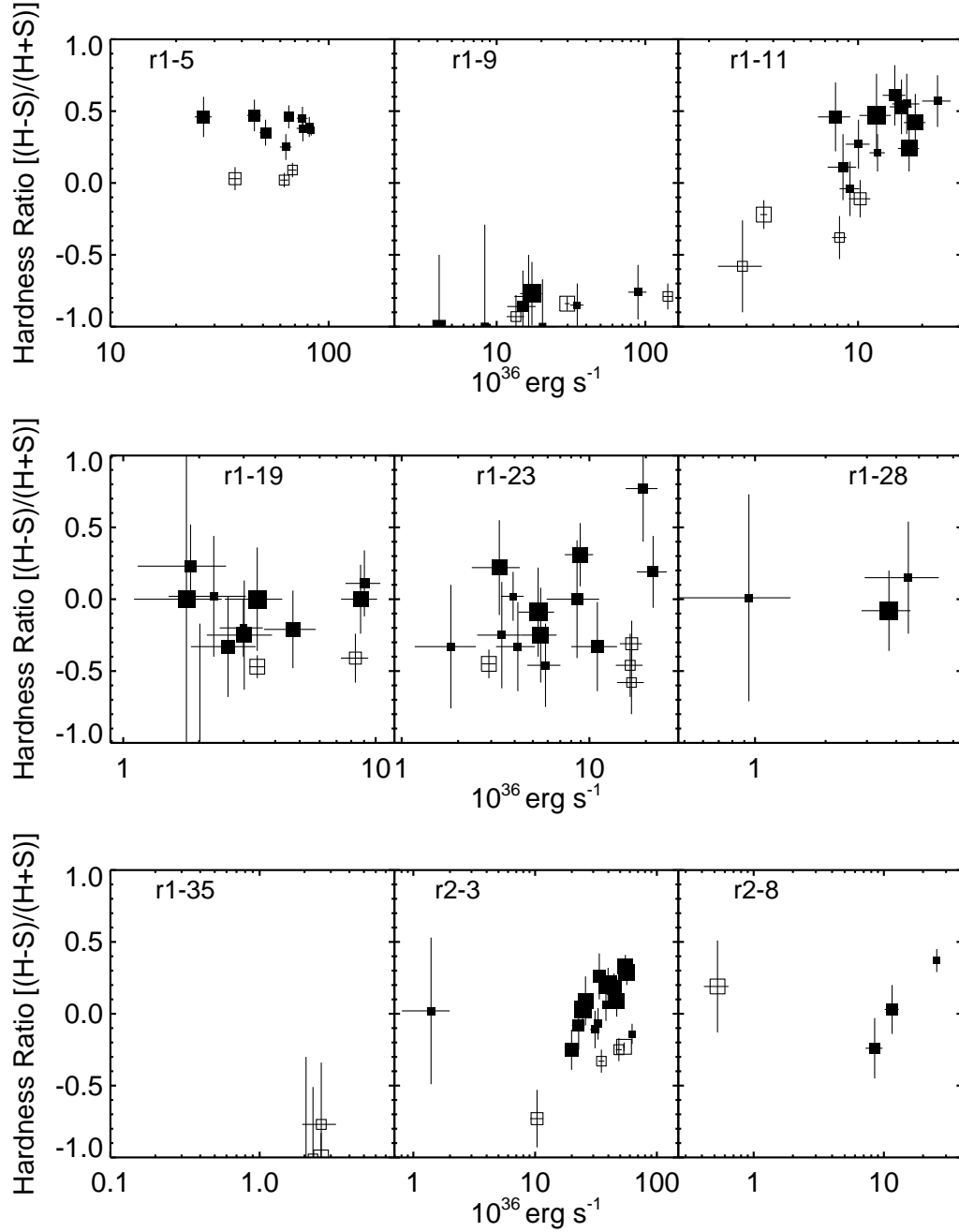


Fig. 19.— The hardness-luminosity diagrams for nine transient sources detected 3 or more times with the ACIS detectors. Filled squares are ACIS-I data points and hollow squares are ACIS-S data points. The luminosities are absorption corrected 0.1–10 keV luminosities measured using the most contemporaneous spectral fit available, and the hardness ratios $[(H-S)/(H+S)]$ are from background-subtracted source counts in 2 bands: S (0.3–1.0 keV) and H (2.0–7.0 keV). The sizes of the data points reflect the times of the observations. Larger data points represent later observations.

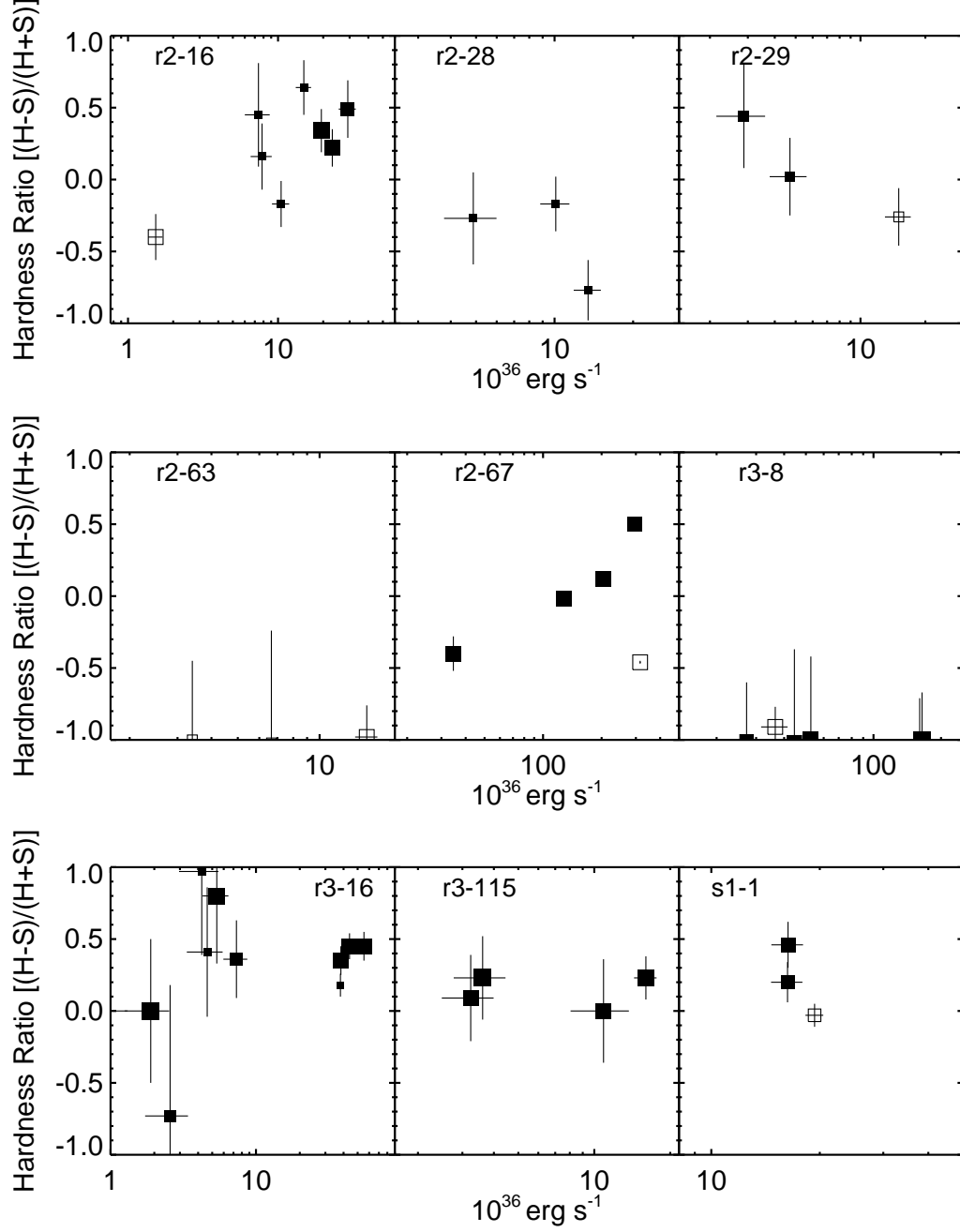


Fig. 20.— The hardness-luminosity diagrams for nine more transient sources detected 3 or more times with the ACIS detectors. Data representation is identical to that in Figure 19.

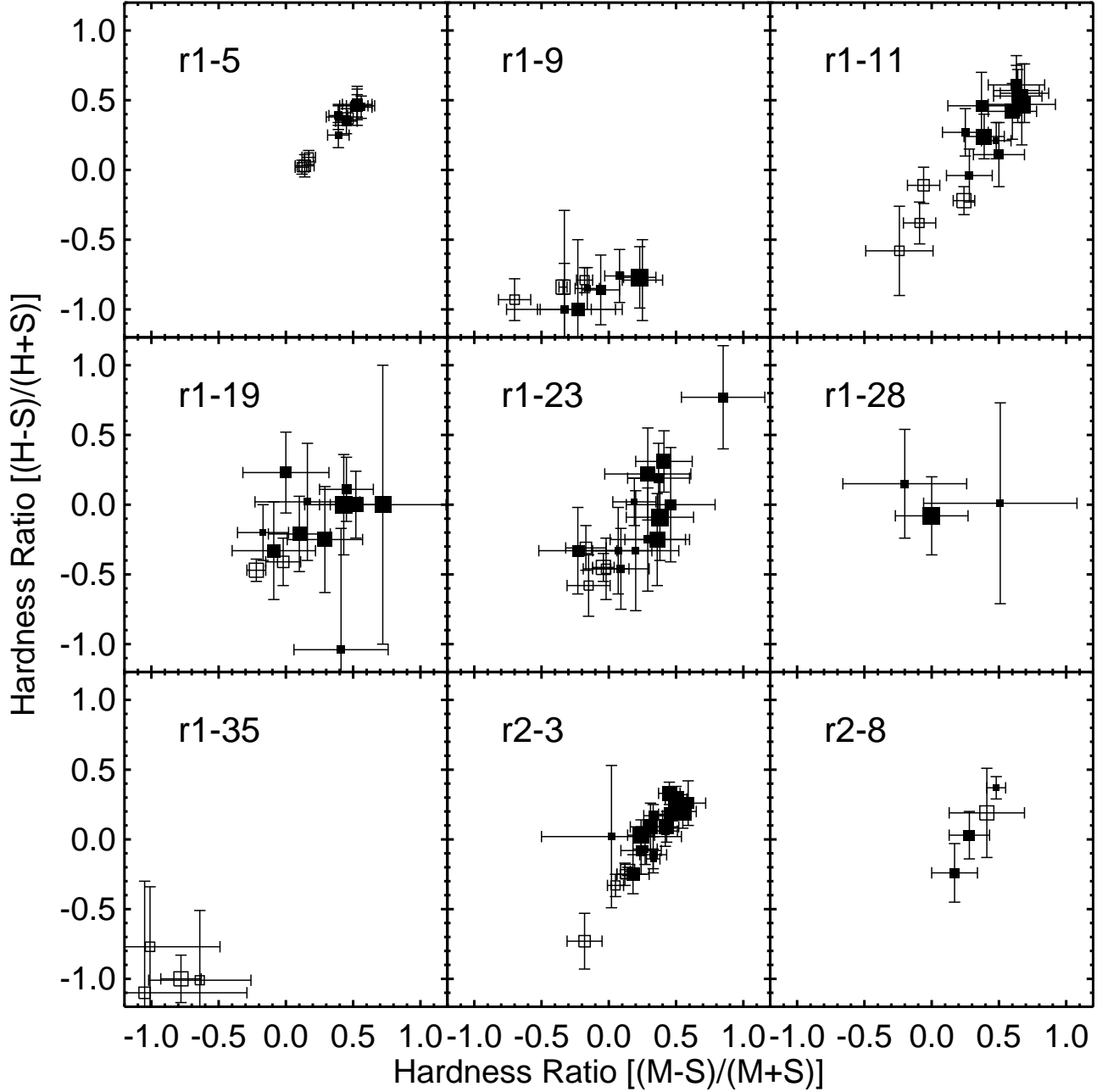


Fig. 21.— The color-color diagrams for nine transient sources detected 3 or more times with the ACIS detectors. Filled squares are ACIS-I data points and hollow squares are ACIS-S data points. The hardness ratios are from background-subtracted source counts in 2 bands: S (0.3–1.0 keV) and H (2.0–7.0 keV). The sizes of the data points reflect the times of the observations. Larger data points represent later observations.

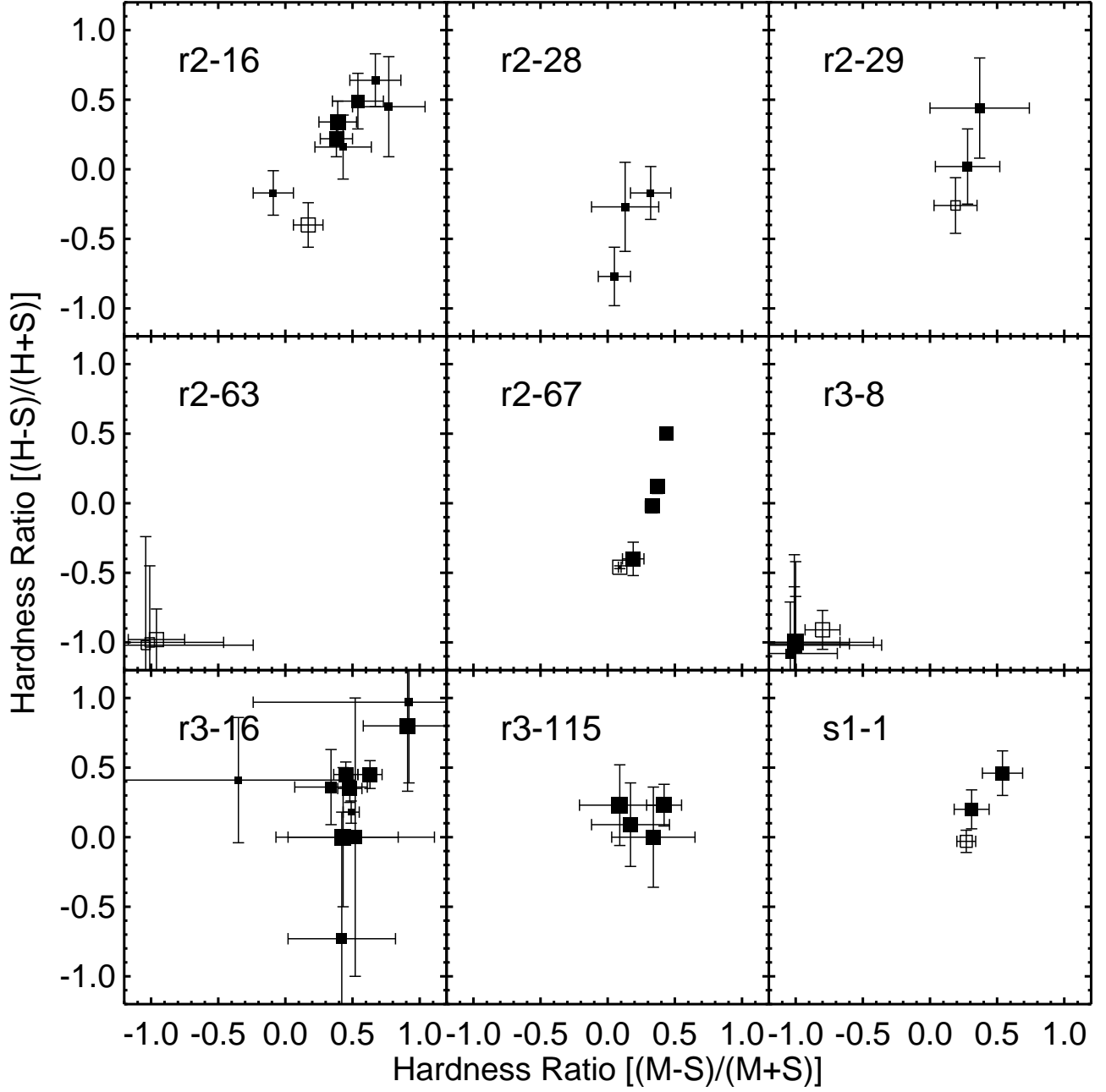


Fig. 22.— The color-color diagrams for nine transient sources detected 3 or more times with the ACIS detectors. Data representation is identical to that in Figure 21.